ENGINEERING OF BIOMATERIALS

INŻYNIERIA BIOMATERIAŁÓW

JOURNAL OF POLISH SOCIETY FOR BIOMATERIALS AND FACULTY OF MATERIALS SCIENCE AND CERAMICS AGH-UST
CZASOPISMO POLSKIEGO STOWARZYSZENIA BIOMATERIAŁÓW I WYDZIAŁU INŻYNIERII MATERIAŁOWEJ I CERAMIKI AGH

Number 144
Numer 144
Volume XXI
Rok XXI

JANUARY 2018
STYCZEŃ 2018

ISSN 1429-7248

PUBLISHER:
WYDAWCA:

Polish Society for Biomaterials in Krakow
Polskie Stowarzyszenie Biomateriałów w Krakowie

ADDRESS OF EDITORIAL OFFICE:
ADRES REDAKCJI:

AGH-UST
30/A3, Mickiewicz Av.
30-059 Krakow, Poland
Akademia Górniczo-Hutnicza
al. Mickiewicza 30/A-3
30-059 Kraków

Issue: 250 copies
Nakład: 250 egz.

Scientific Publishing House AKAPIT
Wydawnictwo Naukowe AKAPIT
e-mail: wn@akapit.krakow.pl

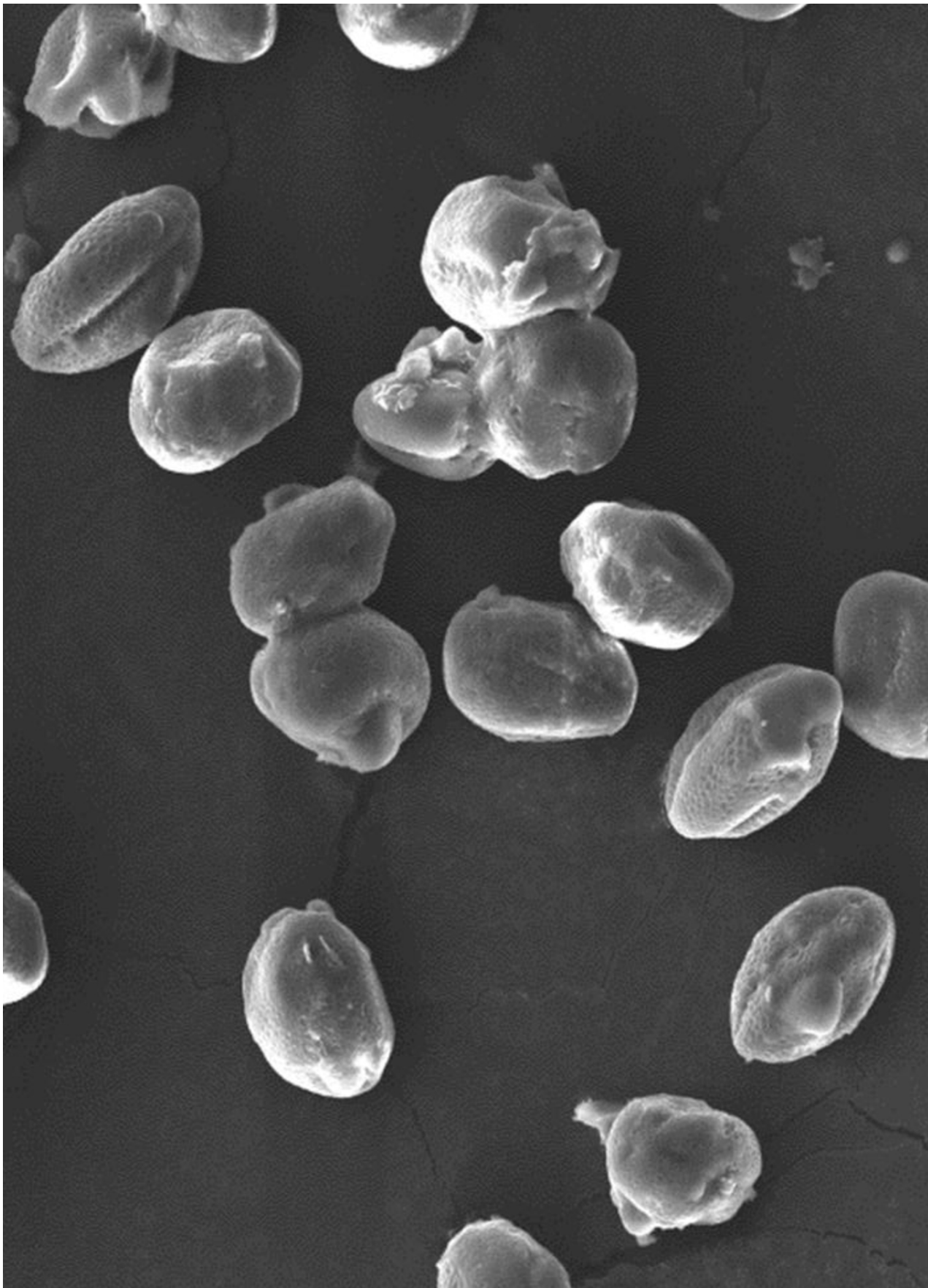

ENGINEERING OF BIOMATERIALS

EDITORIAL BOARD
KOMITET REDAKCYJNY

INTERNATIONAL EDITORIAL BOARD
MIĘDZYNARODOWY KOMITET REDAKCYJNY

ENGINEERING OF BIOMATERIALS

Wskazówki dla autorów

1. Prace do opublikowania w kwartalniku „Engineering of Biomaterials / Inżynieria Biomateriałów" przyjmowane będą wyłącznie w języku angielskim. Możliwe jest również dołączenie dodatkowo polskiej wersji językowej.
2. Wszystkie nadsyłane artykuły są recenzowane.
3. Materiały do druku prosimy przysyłać na adres e-mail: kabe@agh.edu.pl.
4. Struktura artykułu:
• TYTUŁ • Autorzy i instytucje • Streszczenie (200-250 słów) • Słowa kluczowe (4-6) • Wprowadzenie • Materiały i metody • Wyniki i dyskusja • Wnioski • Podziękowania • Piśmiennictwo
5. Autorzy przesyłają pełną wersję artykułu, łącznie z ilustracjami, tabelami, podpisami i literaturą w jednym pliku. Artykuł w tej formie przesyłany jest do recenzentów. Dodatkowo autorzy proszeni są o przesłanie materiałów ilustracyjnych (rysunki, schematy, fotografie, wykresy) w oddzielnych plikach (format np. .jpg, .gif., .tiff, .bmp). Rozdzielczość rysunków min. 300 dpi. Wszystkie rysunki i wykresy powinny być czarno-białe lub w odcieniach szarości i ponumerowane cyframi arabskimi. W tekście należy umieścić odnośniki do rysunków i tabel. W przypadku artykułów dwujęzycznych w tabelach i na wykresach należy umieścić opisy polskie i angielskie.
6. Na końcu artykułu należy podać wykaz piśmiennictwa w kolejności cytowania w tekście i kolejno ponumerowany.
7. Redakcja zastrzega sobie prawo wprowadzenia do opracowań autorskich zmian terminologicznych, poprawek redakcyjnych, stylistycznych, w celu dostosowania artykułu do norm przyjętych w naszym czasopiśmie. Zmiany i uzupełnienia merytoryczne będą dokonywane w uzgodnieniu z autorem.
8. Opinia lub uwagi recenzentów będą przekazywane Autorowi do ustosunkowania się. Nie dostarczenie poprawionego artykułu w terminie oznacza rezygnację Autora z publikacji pracy w naszym czasopiśmie.
9. Za publikację artykułów redakcja nie płaci honorarium autorskiego.
10. Adres redakcji:

Czasopismo
„Engineering of Biomaterials / Inżynieria Biomateriałów"
Akademia Górniczo-Hutnicza im. St. Staszica
Wydział Inżynierii Materiałowej i Ceramiki
al. Mickiewicza 30/A-3, 30-059 Kraków
tel. (48) 12 617 25 03, 12 617 25 61
tel./fax: (48) 12 617 45 41
e-mail: chlopek@agh.edu.pl, kabe@agh.edu.pl

Szczegółowe informacje dotyczące przygotowania manuskryptu oraz procedury recenzowania dostępne są na stronie internetowej czasopisma:
www.biomat.krakow.pl

Warunki prenumeraty

Zamówienie na prenumeratę prosimy przesyłać na adres:
mgr inż. Augustyn Powroźnik
apowroz@agh.edu.pl, tel/fax: (48) 12 617 45 41
Cena pojedynczego numeru wynosi 20 PLN
Konto: Polskie Stowarzyszenie Biomateriałów
30-059 Kraków, al. Mickiewicza 30/A-3
ING Bank Śląski S.A. O/Kraków
nr rachunku 63 1050 1445 1000 0012 0085 6001

Prenumerata obejmuje 4 numery regularne i nie obejmuje numeru specjalnego (materiały konferencyjne).

Instructions for authors

1. Papers for publication in quarterly journal „Engineering of Biomaterials / Inżynieria Biomateriałów" should be written in English.
2. All articles are reviewed.
3. Manuscripts should be submitted to editorial office by e-mail to kabe@agh.edu.pl.
4. A manuscript should be organized in the following order:
• TITLE • Authors and affiliations • Abstract (200-250 words) • Keywords (4-6) • Introduction • Materials and Methods • Results and Discussions • Conclusions • Acknowledgements • References
5. All illustrations, figures, tables, graphs etc. preferably in black and white or grey scale should be additionally sent as separate electronic files (format .jpg, .gif., .tiff, .bmp). High-resolution figures are required for publication, at least 300 dpi. All figures must be numbered in the order in which they appear in the paper and captioned below. They should be referenced in the text. The captions of all figures should be submitted on a separate sheet.
6. References should be listed at the end of the article. Number the references consecutively in the order in which they are first mentioned in the text.
7. The Editors reserve the right to improve manuscripts on grammar and style and to modify the manuscripts to fit in with the style of the journal. If extensive alterations are required, the manuscript will be returned to the authors for revision.
8. Opinion or notes of reviewers will be transferred to the author. If the corrected article will not be supplied on time, it means that the author has resigned from publication of work in our journal.
9. Editorial does not pay author honorarium for publication of article.
10. Address of editorial office:

Journal
„Engineering of Biomaterials / Inżynieria Biomateriałów"
AGH University of Science and Technology
Faculty of Materials Science and Ceramics
30/A-3, Mickiewicz Av., 30-059 Krakow, Poland
tel. (48) 12) 617 25 03, 12 617 25 61
tel./fax: (48) 12 617 45 41
e-mail: chlopek@agh.edu.pl, kabe@agh.edu.pl

Detailed information concerning manuscript preparation and review process are available at the journal's website:
www.biomat.krakow.pl

Subscription terms

Contact:
MSc Augustyn Powroźnik,
e-mail: apowroz@agh.edu.pl
Subscription rates:
Cost of one number: 20 PLN
Payment should be made to:
Polish Society for Biomaterials
30/A3, Mickiewicz Av.
30-059 Krakow, Poland
ING Bank Slaski S.A.
account no. 63 1050 1445 1000 0012 0085 6001

Subscription includes 4 issues and does not include special issue (conference materials).

ISBPPB 2018

4th International Conference on

Biomedical Polymers & Polymeric Biomaterials

15–18 July 2018, Kraków, POLAND

Organizers:

Polish Society for Biomaterials

Faculty of Materials Science and Ceramics, AGH-UST

International Society for Biomedical Polymers and Polymeric Biomaterials

www.isbppb2018.org

27th Biomaterials in Medicine and Veterinary Medicine Annual Conference

11 – 14 October 2018 Rytro, Poland

SAVE THE DATE

11-14

OCTOBER

2018

www.biomat.agh.edu.pl

REGISTER AND SUBMIT AN ABSTRACT

SPIS TREŚCI
CONTENTS

Wersja papierowa czasopisma „Engineering of Biomaterials / Inżynieria Biomateriałów" jest jego wersją pierwotną
Printed version of „Engineering of Biomaterials / Inżynieria Biomateriałów" is a primary version of the journal

PLANT-DERIVED RHAMNOGALACTURONAN-I'S MODULATE PROINFLAMMATORY CYTOKINE GENE EXPRESSION IN NEUTROPHILS STIMULATED BY *E. COLI* LPS AND *P. GINGIVALIS* BACTERIA

Justyna Folkert[1]*, Anna Mieszkowska[1], Bernard Burke[2], Owen Addison[3], Katarzyna Gurzawska[3]

[1] Environmental Biotechnology Department,
Faculty of Energy and Environmental Engineering,
Silesian University of Technology,
44-100 Gliwice, Poland
[2] Faculty of Health & Life Sciences,
University of Coventry, 20 Whitefriars Street,
Coventry CV1 2DS, United Kingdom
[3] Birmingham Dental School and Hospital,
University of Birmingham, 5 Mill Poll Way,
Edgbaston, Birmingham B5 7EG, United Kingdom
*e-mail: justyna.folkert@gmail.com

Abstract

Titanium dental implants often induce the foreign body immune response. The duration of the inflammatory process determines the initial stability and biocompatibility of the implant. The challenge for bone tissue engineering is to develop implant biocompatible and bioactive surface coatings that regulate the inflammatory response and enhance osseointegration. Pectins, plant-derived polysaccharides, have been shown to be potential candidates for surface coating due to their possible roles in improving osseointegration and bone healing.

The aim of this study was to evaluate in vitro the effect of plant-derived pectin rhamnogalacturonan-I (RG-I) nanocoating on pro- and anti-inflammatory human polymorphonuclear leucocytes (PMN) responses to E. coli LPS or P. gingivalis bacteria.

In this study unmodified RG-I and structurally modified RG-I from potato were examined. All in vitro studies were performed on tissue culture polystyrene surfaces (TCPS) or titanium (Ti) discs coated with unmodified and modified RG-Is. Changes in PMN gene expression occurred on both surfaces. The presence of RG-Is down-regulated proinflammatory genes, IL1B, IL8, TNFA. Our results clearly showed that pectin RG-I nanocoating decreased the level of proinflammatory genes expression in stimulated PMN and may therefore be considered as a potential candidate for modulation of the inflammatory response elicited by insertion of implants into living tissue.

Keywords: *pectin, PMN, proinflammatory cytokines, gene expression*

[Engineering of Biomaterials 144 (2018) 2-7]

Introduction

The initial reaction following implant insertion into bone is an inflammatory response [1-4]. PMN (polymorphonuclear leucocytes) represent the first line of the innate immune defence and are abundant in the peri-implant tissues following implant placement. PMN are recruited to the site of injury (associated with implant insertion) and mediate bactericidal activity via phagocytosis, NETosis, and degranulation, alongside secretion of chemokines/cytokines [2,5,6].

The failure of implant treatment is often caused by bacteria infection due to uncontrolled disease such as periodontitis, associated with chronic inflammation [7-9]. *Porhyromonas gingivalis (P. gingivalis), Tannerella forsythia* and *Treponema denticola* represent the periodontal pathogens equipped with a broad array of virulence factors [8]. Unfortunately, the inflammatory mediators produced by PMNs in response to infection can result in host tissue damage and degradation of implant material surfaces [4-6,10]. An excessive influx of PMNs, or their subsequent persistence can therefore lead to impaired wound healing [11,12].

To prevent hyper-activity and/or hyper-reactivity of PMN in peri-implant tissues, a new direction in tissue engineering is to the develop biomaterials that modulate the inflammatory response in their local environment and enhance osseointegration. Plant-derived pectins have been proposed as potential candidates for surface nanocoating of medical devices due to their osteogenic and anti-inflammatory properties [13-22]. In addition their structure can be easily manipulated allowing them to be presented in a range of forms with different biochemical properties [14,15,19]. A number of studies have investigated the effect of pectin polysaccharides, mainly Rhamnogalacturonan-I (RG-I), composed of a backbone of alternating rhamnose and galacturonic acid residues, while arabinian, galactan, and arabino-galactan side chains are presented on the rhamnosyl residues [13-16]. RG-I has been shown to stimulate adhesion, proliferation, differentiation of macrophages [17], fibroblasts [21,22], osteoblasts [15,16,18,19], and bone marrow mesenchymal stem cells [23,30]. In addition, the surface modification of titanium with RG-I has been shown to increase osteoblast mineralization and expression of genes involved in extracellular matrix (ECM) formation, maturation and mineralization [15,16,23,24]. Recently, it has been reported that RG-I may also possess anti-inflammatory properties [17,25-29]. Our previous studies have demonstrated that gene expression of pro-inflammatory cytokines (*Il1b*, *Il6,* and *Tnfa*) in osteoblasts culture infected with *P. gingivalis* was down-regulated at surface coated with RG-I [30]. Therefore, our hypothesis is that anti-inflammatory properties of RG-I may inhibit acute inflammatory response initiated with PMN by down-regulation of *IL1b, IL6, TNFA*.

In this study, the gene expression of cytokines in PMN will be determined under two conditions, stimulation with *P. gingivalis,* the major oral pathogen associated with periodontal diseases, and *Escherichia coli* lipopolysaccharide (*E. coli* LPS).

It has been reported, that proinflammatory cytokine response, during *P. gingivalis* and *E.coli* infection is initiated by different toll-like receptors (TLR) [31,32]. The examination of PMN with *P. gingivalis* and *E.coli* stimulation intended to investigate RG-I effect on both independent mechanisms of immune response through TLR.

The aim of this study was to evaluate *in vitro* the effect of RG-I surface nanocoating on pro- and anti-inflammatory gene expression in human PMN stimulated by *E. coli* LPS or *P. gingivalis* bacteria. This investigation will examine the possibility of modulating *in vitro* PMN proinflammatory activity by RG-Is.

Materials and Methods

Isolation, modification and nanocoating of RG-Is on polystyrene and titanium surfaces

RG-I was prepared as described previously by Gurzawska et al. by treatment of potato pulp (P) with enzyme preparations [15,16]. The chemical properties, monosaccharide composition and linkage analysis of PU (unmodified) and PA (modified) RG-I's have been reported in our previous studies [16]. Briefly, the results showed higher amount of 1,4-galactose in PA compared to PU. To evaluate the *in vitro* effect of a RG-I pectin nanocoating on human PMN responses, two different types of material surfaces were used. Tissue Polystyrene Culture Plates (TCPS) (Techno Plastic Product) with a diameter of 60 mm and commercially pure (grade 2) machined titanium (Ti discs) (Dentsply, Sweden) with a diameter of 60 mm, were prepared. Discs were sterilized by autoclaving for 20 min at 121°C and placed in 6-well TCPS. Adherently, PU and PA RG-I's (128 µg/mL) were coated on surface of 6-well TCPS and on the surface of Ti discs. The reaction was carried out at room temperature overnight in sterile conditions on a shaker (IKA-Werke GmbH & Co. KG) at 100 rpm. After coating the TCPS plates and Ti discs were rinsed extensively in sterile deionised water and then allowed to air dry in a laminar flow hood before *in vitro* experiments.

In vitro studies

TCPS and Ti discs with PU and PA nanocoatings were tested, and compared with control uncoated TCPS and uncoated Ti discs. Peripheral blood for PMN isolation for all *in vitro* experiments was collected from healthy volunteer donors (n = 3). Written informed consent was obtained from all volunteer donors and the study was approved by the local research ethics committee of the Dental School, College of Medical and Dental Sciences, University of Birmingham, Birmingham, UK (approval number 14/SW/1148).

Cell culture

PMNs were isolated from heparinised (17 IU/mL) peripheral blood using Percoll density gradients (GE Healthcare) as previously described [33]. Briefly, two discontinuous gradients, 1.079 and 1.098, were used for PMN isolation with concomitant erythrocyte lysis (0.83% NH_4Cl containing 1% $KHCO_3$, 0.04% EDTA and 0.25% BSA). Isolated cells were resuspended in PBS. Cell viability, typically >98%, was determined by dye exclusion (trypan blue). PMNs were seeded at a cell density of 1×10^5/mL in RG-Is coated and uncoated 6-well TCPS plates and on RG-Is coated and uncoated Ti discs placed in 6-well TCPS. The cells were incubated for 30 min at 37°C with 5% CO_2.

Cell morphology

The cells incubated for 30 min on uncoated and coated Ti disc were observed with scanning electron microscope (SEM) (ZEISS). The PMN were fixed with 2-2.5% glutaraldehyde (Biochrom), following rinsing thrice with PBS. After dehydration with 30%, 40%, 50%, 60%, 70%, 90%, 95% and 100% ethanol for 5 min, respectively, the hexamethyldisilazane (HMDS) was added to samples and left to evaporate. After drying, samples were mounted and placed in a scanning electron microscope operating at 10 kV and using secondary electron imaging mode. The TCPS has been covered with gold layer, however the Ti surface did not required gold coating.

E. coli LPS stimulation and P. gingivalis invasion/infection assay

For the bacterial exposure assay, *P. gingivalis* strain (*Pg*; ATCC 33277) was prepared as previously described [9]. The bacteria were harvested by centrifugation, washed and resuspended in PBS and heat treated for 10 min at 100°C. The number of bacteria was determined by measuring the OD at 600 nm and appropriate dilutions were made to obtain the desired multiplicity of infection (MOI).

After 30 min incubation PMN were treated with *E. coli* serotype O26:B6 LPS (Sigma-Aldrich L5543; Sigma-Aldrich) at 100 ng/ml or heat-killed *P. gingivalis* bacteria at a multiplicity of infection of 100 bacteria per PMN. PMN were cultured in the presence of *E. coli* LPS or *P. gingivalis* for 4 h at 37°C with 5% CO_2 prior to RNA isolation.

RNA isolation and real-time RT-PCR

RNA was isolated from PMN using TRI reagent (Sigma) and the Qiagen RNeasy Mini Kit according to the manufacturer's instructions, and was quantified by UV spectrometry at 260 nm (Eppendorf). Isolated RNA was reverse transcribed using a one-step high capacity cDNA reverse transcription (RT) kit (Applied Biosystems). The comparative $2^{-\Delta\Delta Ct}$ method was used to quantify relative gene expression [38]. Relative expression levels were calculated for each sample after normalization against the housekeeping gene *B2M*. The calibrator was a pool of the cDNA synthesized from total-RNA isolated from PMN. A LightCycler 480 SYBR Green I Master Real Time PCR instrument (Roche Diagnostics GmbH) was used for quantification of target genes: tumour necrosis factor-alpha (*TNFA*), interleukin-1 beta (*IL1B*), interleukin-8 (*IL8*), interleukin-10 (*IL10*) and beta-2-microglobulin (*B2M*). The primer (Sigma) sequences are described in TABLE 1. 1 µL of cDNA and 9 µL of reaction mix was used in each well of a 96-well plate (Roche), according to the manufacturer's instructions. The PCR reaction conditions were 95°C for 5 min, followed by 40 cycles of 10 s at 95°C; 15 sec at 62,3°C; 20 s at 72°C and a final cycle of 20 min with increasing temperature from 60°C to 95°C, followed by the standard denaturation curve.

TABLE 1. Primer sequences used for Real-time PCR.

Target gene	Primer	Sequence 5' to 3'
B2M	forward	ACCCCCACTGAAAAAGATGA
	reverse	ATCTTCAAACCTCCATGATG
TNFA	forward	ATCCTGGGGGACCCAATGTA
	reverse	AAAAGAAGGCACAGAGGCCA
IL1B	forward	TTCGAGGCACAAGGCACAA
	reverse	AAGTCATCCTCATTGCCACTGT
IL8	forward	CTCCTTGGCAAAACTGCACC
	reverse	CAGAGACAGCAGAGCACACA
IL10	forward	TGCCTTCAGCAGAGTG
	reverse	GGGAAGAAATCGATGA

Statistical analyses

Descriptive statistics were used and mean values were calculated. Data are shown as mean ± SEM and were analysed using one-way ANOVA and post hoc Bonferroni test (IBM SPSS Statistic 22). A significance level of p value = 0.05 was used throughout the study.

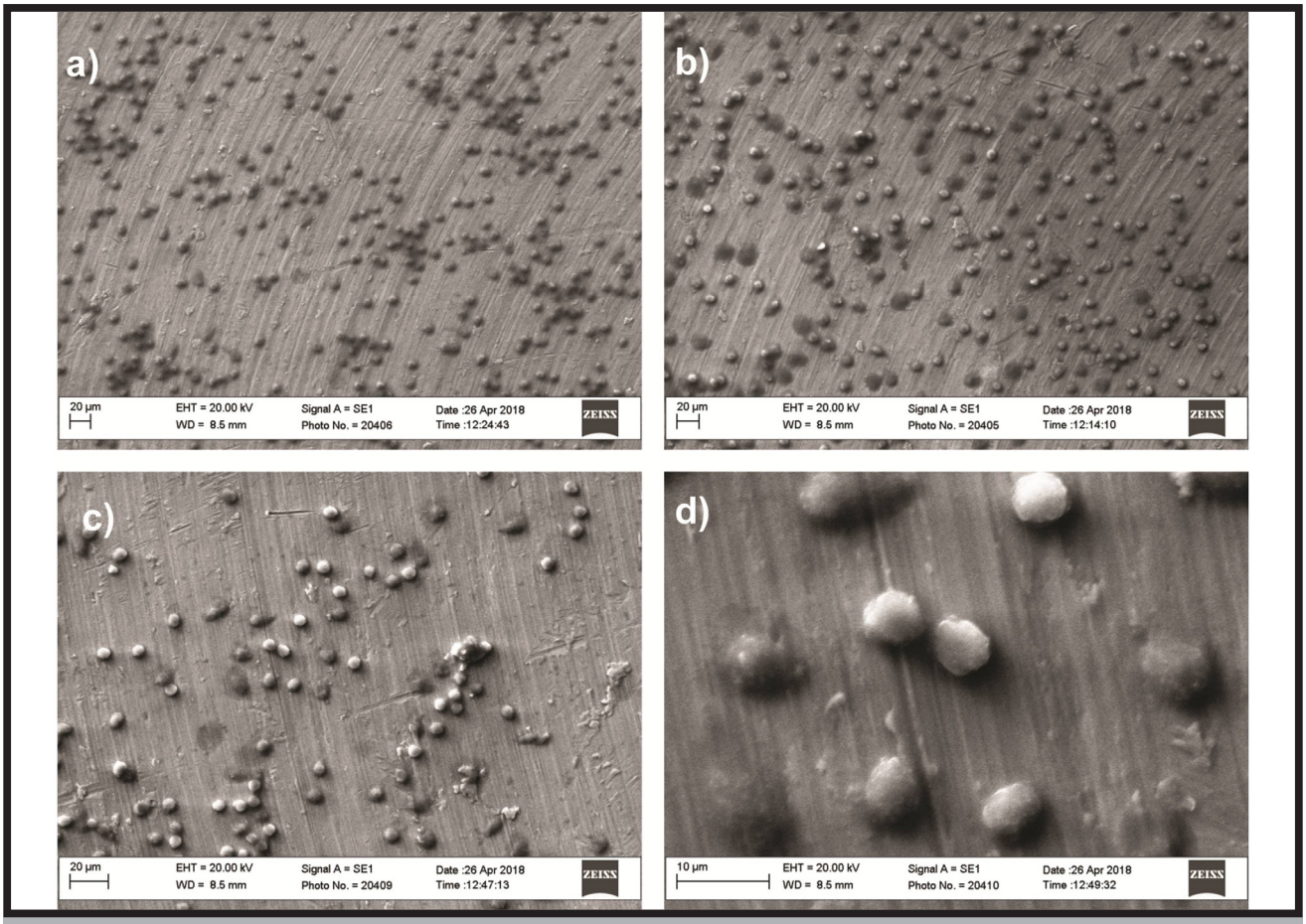

FIG. 1. Representative images of PMN seeded on titanium (Ti) discs (a) without coating (C), Ti discs coated (b) with unmodified pectin RG-I (PU), and Ti discs coated (c, d) with dearabinanated pectin RG-I (PA) performed with scanning electron microscope.

Results

PU and PA coating do not influence PMN attachment

Analysis of PMN morphology on uncoated and coated Ti discs, via scanning electron microscopy, showed some cells onto both surfaces (FIG. 1). PMN isolated from blood were similar in size, about 6-7 µm in diameter. SEM demonstrated that PMN were round-shaped. No differences in cell morphology as well as cell spreading were found between control and PU, PA.

Influence of PU and PA coating on PMN gene expression on tissue culture polystyrene surfaces

The effect of PU and PA RG-I coatings on gene expression in PMN cultured on TCPS surfaces was investigated using Real-Time RT-PCR. The level of pro-inflammatory *TNFA, IL1B, IL8*, and anti-inflammatory *IL10* gene expression was modified by RG-I in PMN stimulated with *E. coli* LPS or *P. gingivalis* bacteria and also unstimulated PMN. The results are shown in FIG. 2.

In general, pro-inflammatory *TNFA, IL1B, IL8* expression in PMN was the highest on control TCPS surfaces and the lowest on PA coated surfaces. PA significantly decreased *IL1B* ($p < 0.05$) and *IL8* ($p < 0.001$) expression in *P. gingivalis* stimulated PMN compared to control, uncoated TCPS. In normal conditions, without LPS *E. coli* and *P. gingivalis*, the *IL8* expression in unstimulated cells was significantly lower on PU ($p<0.01$) and PA ($p<0.001$) compared with TCPS control. No differences of *TNFA* gene expression were observed in both stimulated and unstimulated PMN cultured on PU and PA coated surfaces compared with the TCPS control.

The results of *IL-10* gene expression in stimulated and unstimulated PMN showed that there was no significant difference between PU, PA and control.

Generally, the level of *TNFA, IL1B, IL8*, and *IL10* expression was higher in PMN stimulated with *E. coli* LPS than with *P. gingivalis*. The lowest level of gene expression was observed in unstimulated PMN.

PU and PA coating influence PMN gene expression on titanium surfaces

Gene expression of *TNFA, IL1B, IL8* and *IL10* was detected in *E. coli* LPS/ *P. gingivalis* stimulated PMN and in unstimulated PMN cultured on Ti surfaces without PU/PA coatings. The results are shown in FIG. 3.

Generally, pro-inflammatory *TNFA, IL1B, IL8* expression in PMN stimulated with *P. gingivalis* or LPS *E. coli* were the highest on control titanium surfaces and the lowest on PA coated surfaces. PA and PU significantly decreased *TNFA* ($p < 0.001$) and *IL8* ($p < 0.001$) expression in *P. gingivalis* stimulated PMN compared with the Ti control. The *IL1B* expression in cells activated with *P. gingivalis* was significantly decreased by PA ($p < 0.001$).

No significant differences of anti-inflammatory *IL-10* gene expression were observed in both stimulated and unstimulated PMN grown on PU and PA coated compared with Ti control surfaces.

In LPS *E. Coli* stimulated conditions on Ti surface, similar to TCPS surface it has been observed, a higher pro-inflammatory gene expression compared to *P. gingivalis* stimulated PMN and unstimulated PMN, respectively.

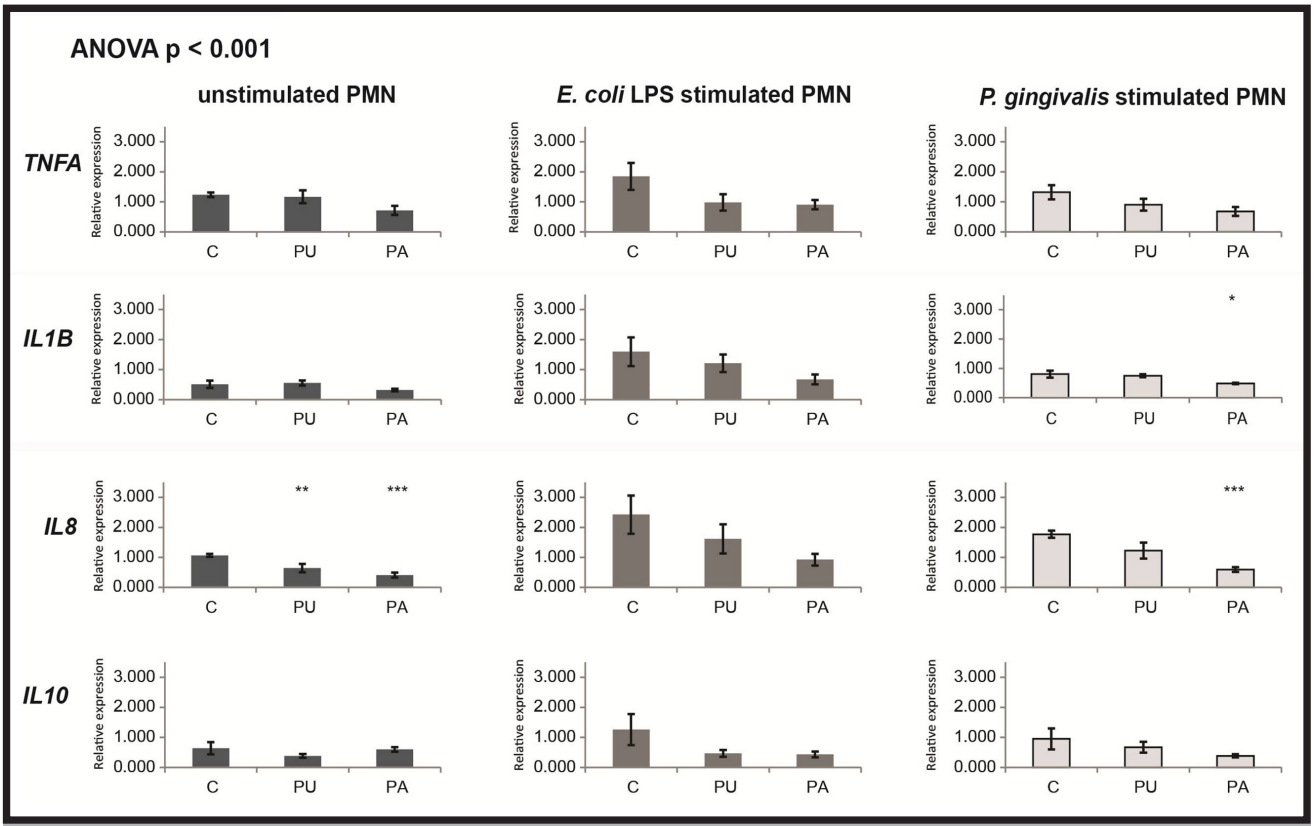

FIG. 2. Gene expression of PMN seeded on tissue culture polystyrene surface (TCPS) without coating (C), TCPS coated with unmodified pectin RG-I (PU), and TCPS coated with dearabinanated pectin RG-I (PA) as assessed by Real-Time RT-PCR measurement of *TNFA, IL1B, IL8,* and *IL10* genes after 4 h. Data are given as means +/- SEM (n = 6) and were statistically analysed using one-way ANOVA with Bonferroni's for multiple comparisons (p-values: * p < 0.05; ** p < 0.01; *** p < 0.001).

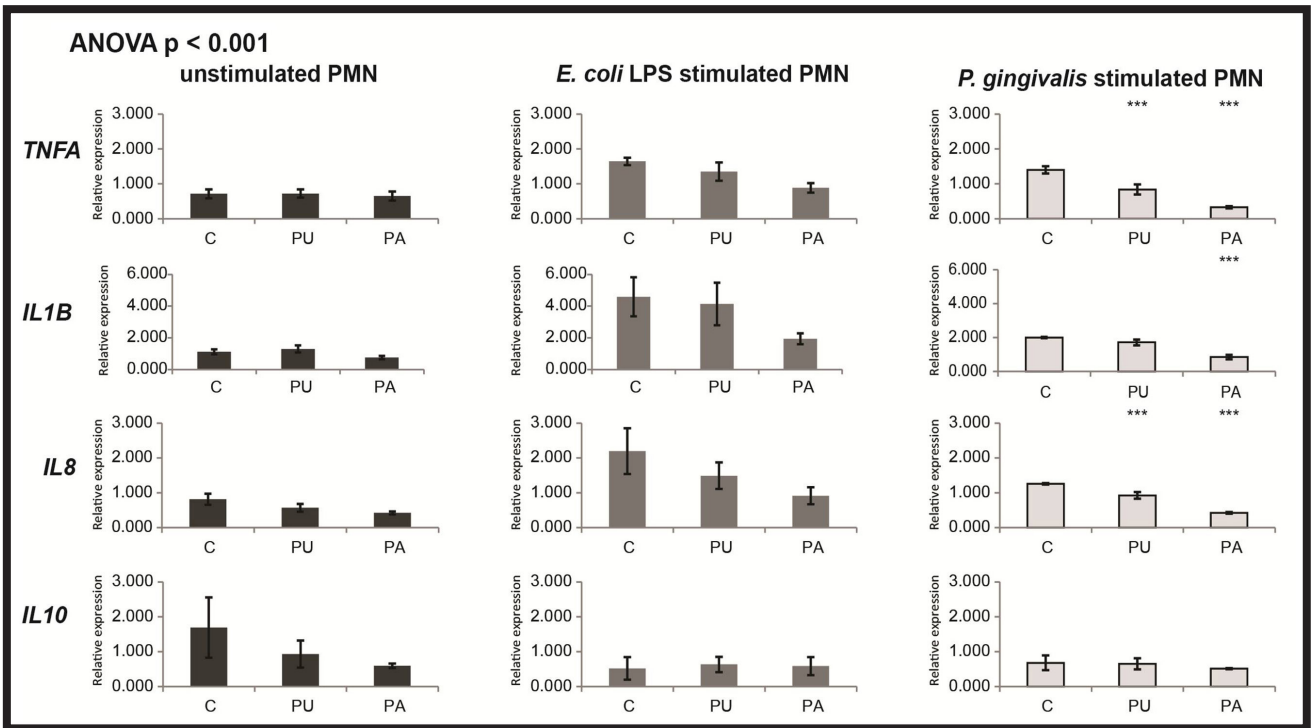

FIG. 3. Gene expression of PMN seeded on titanium (Ti) discs without coating (C), Ti discs coated with unmodified pectin RG-I (PU), and Ti discs coated with dearabinanated pectin RG-I (PA) as assessed by Real-Time RT-PCR measurement of *TNFA, IL1B, IL8,* and *IL10* genes after 4 h. Data are given as means +/- SEM (n = 6) and were statistically analysed using one-way ANOVA with Bonferroni's for multiple comparisons (p-values: * p < 0.05; ** p < 0.01; *** p < 0.001).

Discussions

In the present study we assessed the effect of plant-derived pectin Rhamnogalacturonan-I (RG-I) nanocoating on the gene expression of pro-inflammatory cytokines (*IL1B*, *IL8,* and *TNFA*) and anti-inflammatory cytokine (*IL10*) in human PMN responses. Nanocoating with RG-I did not changed significantly the cytokine gene expression in PMN culture under *E. coli* LPS compared to control. However, in PMN infected with *P. gingivalis* the gene expression of *IL1B, TNFA* and *IL8* was significantly down-regulated on surfaces coated with galactose rich RG-I (PA), suggesting reduction of inflammation.

In general, the difference between the unmodified (PU) and modified (PA) RG-Is was reflected by the sugar composition [16]. The PA has shorter arabinose side chains compare with PU, that made galactose side chains exposed to direct cell interaction. A number of studies [34-37] have shown direct interaction of galactose with Galectin-3 (Gal-3), a glycan-binding protein composed of a single carbohydrate-recognition domain (CRD) and an N-terminal aggregation domain [34-37]. Gal-3 is up-regulated during inflammation, induced by bacteria infection [38,39] and is predominantly expressed by innate cells, mast cells, neutrophils and eosinophils [36]. Gal-3 was reported to favour neutrophil recruitment and activation [37]. Therefore, the mechanism of RG-I interaction with Gal-3 has to be investigated in further studies, where Gal-3 gene expression and extracellular level should be measured.

On the cell level, we have demonstrated that nanocoatings with PU and PA have no effect on PMN morphology.

Furthermore, we investigated pro- and anti-inflammatory gene expression in PMN stimulated with LPS *E. coli* or *P. gingivalis* bacteria compared to unstimulated PMN on two types of surfaces: tissue culture polystyrene surfaces (TCPS) and titanium (Ti) discs. The use of two types of surfaces allows for a more accurate interpretation of *in vitro* results and prediction of surface-PMN cell interaction during initial stage of osseointegration. Our results showed differences between cytokine gene expression on titanium compared to TCPS, what indicates that the physical properties, such as roughness may affect cell response. Similar observation has been reported in previous work by Gurzawska et. al 2013, where TCPS, titanium discs and Ti implants coated with RG-I were compared. However, on both TCPS and Ti surface the results of the present study showed that presence of RG-Is, especially PA, reduced pro-inflammatory gene expression in *E. coli* LPS/*P.gingivalis* stimulated PMN and unstimulated PMN.

In the current study, we focused on the expression of selected genes reflecting acute inflammation. PMN have the ability to synthesize pro- and anti-inflammatory cytokines and growth factors that modulate the inflammatory response [38,39]. Interleukin-1β, interleukin-8, and tumour necrosis factor-α are pro-inflammatory cytokines playing crucial role in inflammatory process [38] and destructive effects on bone [12]. TNF-α, IL-1 and other pro-inflammatory cytokines determinate an inflammatory response on the foreign body that can cause severe tissue damage and premature failure of implanted materials [12]. In this study, we demonstrate that RG-I nanocoating influenced the pro-inflammatory genes expression, leading to *IL1B*, *IL8* and *TNFA* down-regulation in unstimulated and stimulated PMN. Lower activity of unstimulated PMN on PU and PA indicated that RG-Is did not induce the inflammatory reaction.

Previous *in vitro* studies evaluating the influence of pectin on inflammatory responses investigated mainly pro-inflammatory cytokine levels (IL-6 and TNF-α) [17,29,30]. In this study we assessed not only PMN pro-inflammatory, but also anti-inflammatory gene expression. PMN produce anti-inflammatory cytokines, such as interleukin-10 (IL-10), which plays a crucial role in acute and persistent bacterial infection. This cytokine is responsible for reduction of inflammation by e.g. inhibiting the secretion of pro-inflammatory cytokines, such as TNF-α [42]. In general, our results showed that the level of expression of the anti-inflammatory cytokine *IL10* in unstimulated and stimulated PMNs on surfaces coated with PU and PA was lower than on controls on polystyrene and titanium surfaces, but no significant differences were observed. Our results are in contrast with research by Ovodova et al. (2011) [43] on male A/HeJ mice showing that the pectic polysaccharide called apiuman isolated from celery stalks improved the survival of mice subjected to a lethal dose of LPS. Apiuman decreased the production of the pro-inflammatory IL-1ß cytokine and increased anti-inflammatory IL-10 cytokine synthesis. The explanation for different biological effect might be due to the differences in sugar composition and side chain structure of PU, PA and apiuman.

Our results indicated that RG-I is capable to reduce pro-inflammatory cytokine expression in *P .gingivalis* stimulated PMN but not after *E. coli* stimulation. This effect may be explained by different mechanism of activation of immune response by these pathogens. Recently it has been reported that *P. gingivalis* LPS activate immune response by TLR2 while LPS of enterobacteria stimulates mainly TLR4 [31,32]. Our observations suggest that the effect of RG-I nanocoating may be related to direct interaction with TLR2, however further studies are necessary to confirm this hypothesis.

In summary, nanocoating with PA, with a higher content of galactose than PU resulted in a lower level of *IL1B*, *IL8* and *TNFA* gene expression in stimulated with *P. gingivalis* PMN compared to PU coating. The results will support further *in vitro* studies to investigate the mechanism of RG-I on activated PMN cells. Our data suggests that RG-I might be promising agent for prevention of implant failure due to acute inflammation.

Conclusions

Modulation of the inflammatory response is a new direction in the field of tissue engineering. The polymorphonuclear leucocytes (PMN) play a key role in preventing infection; however, their excessive activity leads to implant failure. In summary, we have demonstrated that polystyrene and titanium surfaces coated with unmodified (PU) and enzymatically modified (PA) pectin RG-I from potato affected pro-inflammatory gene expression in PMN stimulated with *P. gingivalis*. *IL1B, IL8, TNFA* expressions were down-regulated in stimulated PMN cultured on PA and PU surfaces compared to uncoated TCPS and titanium control surfaces. These results suggest the possibility of using coating with pectin-derived polysaccharides to control inflammation in tissue after implant insertion. Our findings suggest that pectin RG-I has considerable potential to inhibit the inflammatory response and prevent tissue destruction, providing optimal healing and osseointegration.

Acknowledgments

The authors thank RAPID (Rheumatoid Arthritis and Periodontal Inflammatory Disease) research group for valuable assistance and Bodil Jørgensen and Peter Ulvskov from University of Copenhagen for providing RG-Is.

The authors declare that there is no conflict of interest.

References

[1] Anderson J.M., Rodriguez A., Chang D.T.: Foreign body reaction to biomaterials. Seminars in immunology 20(2) (2008) 86-100.
[2] Jhunjhunwala S., Aresta-DaSilva S., Tang K., Alvarez D., Webber M.J., et al.: Neutrophil responses to sterile implant materials. PloS one 10(9) (2015) e0137550.
[3] Vitkov L., Krautgartner W-D., Obermayer A., Stoiber W., Hannig M., et al.: The initial inflammatory response to bioactive implants is characterized by NETosis. PloS one 10(3) (2015) e0121359.
[4] Zhou J., Tsai Y-T., Weng H., Tang E.N., Nair A., et al.: Real-time detection of implant-associated neutrophil responses using a formyl peptide receptor-targeting NIR nanoprobe. International journal of nanomedicine 2012(7) (2012) 2057-2068.
[5] Regan M., Barbul A.: The cellular biology of wound healing. Wound Healing 1 (1994) 3-17.
[6] Lee S.J., Atala A., Yoo J.J.: In Situ Tissue Regeneration: Host Cell Recruitment and Biomaterial Design: Academic Press (2016) 40-44.
[7] Ling M.R., Chapple I., Matthews J.: Peripheral blood neutrophil cytokine hyper-reactivity in chronic periodontitis. Innate immunity 21(7) (2015) 714-725.
[8] Koziel K., Potempa J., Mydel P.: The Link Between Periodontal Disease and Rheumatoid Arthritis: An Updated Current rheumatology reports 16(3) (2014) 408.
[9] Tajima S., Chu J.S.F., Komvopoulos K.: Differential regulation of endothelial cell adhesion, spreading, and cytoskeleton on low-density polyethylene by nanotopography and surface chemistry modification induced by argon plasma treatment. Journal of Biomedical Materials Research Part A 84(3) (2008) 828-836.
[10] Wright H.L., Moots R.J., Bucknall R.C., Edwards S.W.: Neutrophil function in inflammation and inflammatory diseases. Rheumatology 49(9) (2010) 1618-1631.
[11] Wilgus T.A., Roy S., McDaniel J.C.: Neutrophils and wound repair: positive actions and negative reactions. Advances in wound care 2(7) (2013) 379-388.
[12] Mountziaris P.M., Mikos A.G.: Modulation of the inflammatory response for enhanced bone tissue regeneration. Tissue Engineering Part B: Reviews 14(2) (2008) 179-186.
[13] Gurzawska K., Dirscherl K., Yihua Y., Byg I., Bodil J., et al.: Characterization of pectin nanocoatings at polystyrene and titanium surfaces. Journal of Surface Engineered Materials and Advanced Technology 3(04) (2013) 20.
[14] Gurzawska K., Svava R., Jørgensen N.R., Gotfredsen K.: Nanocoating of titanium implant surfaces with organic molecules. Polysaccharides including glycosaminoglycans. Journal of biomedical nanotechnology 8(6) (2012) 1012-1024.
[15] Gurzawska K., Svava R., Syberg S., Yihua Y., Haugshøj K.B., et al.: Effect of nanocoating with rhamnogalacturonan-I on surface properties and osteoblasts response. Journal of Biomedical Materials Research Part A 100(3) (2012) 654-664.
[16] Gurzawska K., Svava R., Yihua Y., Haugshøj K.B., Dirscherl K., et al.: Osteoblastic response to pectin nanocoating on titanium surfaces. Materials Science and Engineering: C 43 (2014) 117-125.
[17] Bussy C., Verhoef R., Haeger A., Morra M., Duval J.L., et al.: Modulating in vitro bone cell and macrophage behavior by immobilized enzymatically tailored pectins. Journal of Biomedical Materials Research Part A 86(3) (2008) 597-606.
[18] Kokkonen H., Cassinelli C., Verhoef R., Morra M., Schols H., et al.: Differentiation of osteoblasts on pectin-coated titanium. Biomacromolecules 9(9) (2008) 2369-2376.
[19] Kokkonen H., Verhoef R., Kauppinen K., Muhonen V., Jørgensen B., et al.: Affecting osteoblastic responses with in vivo engineered potato pectin fragments. Journal of Biomedical Materials Research Part A 100(1) (2012) 111-119.
[20] Morra M.: Biochemical modification of titanium surfaces: peptides and ECM proteins. Eur Cell Mater 12(1) (2006) 15.
[21] Morra M., Cassinelli C., Cascardo G., Nagel M-D., Della Volpe C., et al.: Effects on interfacial properties and cell adhesion of surface modification by pectic hairy regions. Biomacromolecules 5(6) (2004) 2094-2104.
[22] Nagel M-D., Verhoef R., Schols H., Morra M., Knox J.P., et al.: Enzymatically-tailored pectins differentially influence the morphology, adhesion, cell cycle progression and survival of fibroblasts. Biochimica et Biophysica Acta (BBA)-General Subjects 1780(7) (2008) 995-1003.
[23] Folkert J., Meresta A., Gaber T., Miksch K., Buttgereit F., et al.: Nanocoating with plant-derived pectins activates osteoblast response in vitro. International Journal of Nanomedicine 12 (2017) 239.
[24] Svava R., Gurzawska K., Yihau Y., Haugshøj K.B., Dirscherl K., et al.: The structurally effect of surface coated rhamnogalacturonan I on response of the osteoblast-like cell line SaOS-2. Journal of Biomedical Materials Research Part A 102(6) (2014) 1961-1971.
[25] Markov P., Popov S., Nikitina I., Ovodova R., Ovodov Y.S.: Anti-inflammatory activity of pectins and their galacturonan backbone. Russian Journal of Bioorganic Chemistry 37(7) (2011) 817-821.
[26] Popov S., Ovodova R., Popova G.Y., Nikitina I., Ovodov Y.S.: Adhesion of human neutrophils to fibronectin is inhibited by comaruman, pectin of marsh cinquefoil Comarum palustre L., and by its fragments. Biochemistry (Moscow) 70(1) (2005) 108-112.
[27] Popov S., Ovodova R., Popova G.Y., Nikitina I., Ovodov Y.S.: Inhibition of neutrophil adhesion by pectic galacturonans. Russian Journal of Bioorganic Chemistry 33(1) (2007) 175-180.
[28] Popov S., Popova G.Y., Ovodova R., Ovodov Y.S.: Antiinflammatory activity of the pectic polysaccharide from Comarum palustre. Fitoterapia 76(3) (2005) 281-287.
[29] Gallet M., Vayssade M., Morra M., Verhoef R., Perrone S., et al.: Inhibition of LPS-induced proinflammatory responses of J774.2 macrophages by immobilized enzymatically tailored pectins. Acta biomaterialia 5(7) (2009) 2618-2622.
[30] Meresta A., Folkert J., Gaber T., Miksch K., Buttgereit F., et al.: Plant-derived pectin nanocoatings to prevent inflammatory cellular response of osteoblasts following Porphyromonas gingivalis infection. International Journal of Nanomedicine 12 (2017) 433.
[31] Andrukhov O., Ertlschweiger S., Moritz A., Bantleon H.P., Rausch-Fan X.: Different effects of P. gingivalis LPS and E. coli LPS on the expression of interleukin-6 in human gingival fibroblasts. Acta Odontologica Scandinavica 72(5) (2014) 337-345.
[32] Maekawa T., Krauss J.L., Abe T., Jotwani R., Triantafilou M., et al.: Porphyromonas gingivalis manipulates complement and TLR signaling to uncouple bacterial clearance from inflammation and promote dysbiosis. Cell host & microbe 15(6) (2014) 768-778.
[33] Matthews J., Wright H., Roberts A., Cooper P., Chapple I.: Hyperactivity and reactivity of peripheral blood neutrophils in chronic periodontitis. Clinical & Experimental Immunology 147(2) (2007) 255-264.
[34] MacKinnon A.C., Farnworth S.L., Hodkinson P.S., Henderson N.C., Atkinson K.M., et al.: Regulation of alternative macrophage activation by galectin-3. The Journal of Immunology 180(4) (2008) 2650-2658.
[35] Hsu D.K., Yang R.Y., Pan Z., Yu L., Salomon D.R., et al.: Targeted disruption of the galectin-3 gene results in attenuated peritoneal inflammatory responses. The American journal of pathology 156(3) (2000) 1073-1083.
[36] Li Y., Komai-Koma M., Gilchrist D.S., Hsu D.K., Liu F.T., et al.: Galectin-3 is a negative regulator of lipopolysaccharide-mediated inflammation. The Journal of Immunology 181(4) (2008) 2781-2789.
[37] Sato H.: Enzymatic procedure for site-specific pegylation of proteins. Advanced drug delivery reviews, 54(4) (2002) 487-504.
[38] Hatanaka E., Monteagudo P., Marrocos M., Campa A.: Neutrophils and monocytes as potentially important sources of proinflammatory cytokines in diabetes. Clinical & Experimental Immunology 146(3) (2006) 443-447.
[39] Cassatella M.A., Gasperini S., Russo M.P.: Cytokine Expression and Release by Neutrophilsa. Annals of the New York Academy of Sciences 832(1) (1997) 233-242.
[40] Selders G.S., Fetz A.E., Radic M.Z., Bowlin G.L.: An overview of the role of neutrophils in innate immunity, inflammation and host-biomaterial integration. Regenerative Biomaterials 4(1) (2017) 55.
[41] Theilgaard-Mönch K., Knudsen S., Follin P., Borregaard N.: The transcriptional activation program of human neutrophils in skin lesions supports their important role in wound healing. The Journal of Immunology 172(12) (2004) 7684-7693.
[42] Peñaloza H.F., Nieto P.A., Muñoz-Durango N., Salazar-Echegarai F.J., Torres J., et al.: Interleukin-10 plays a key role in the modulation of neutrophils recruitment and lung inflammation during infection by Streptococcus pneumoniae. Immunology 146(1) (2015) 100-112.
[43] Ovodova R.G., Golovchenko V.V., Popov S.V., Popova G.Y., Paderin N.M., et al.: Chemical composition and anti-inflammatory activity of pectic polysaccharide isolated from celery stalks. Food Chemistry 114(2) (2009) 610-615.

ACRYLIC COMPOSITE MATERIALS MODIFIED WITH BEE POLLEN FOR BIOMEDICAL APPLICATION

Wioletta Florkiewicz[1]*, Agnieszka Sobczak-Kupiec[1], Bożena Tyliszczak[2]

[1] Institute of Inorganic Chemistry and Technology, Cracow University of Technology, ul. Warszawska 24, 31-155 Krakow, Poland
[2] Department of Chemistry and Technology of Polymers, Cracow University of Technology, ul. Warszawska 24, 31-155 Krakow, Poland
*e-mail: florkiewicz@chemia.pk.edu.pl

Abstract

The aim of this paper is to present the influence of bee pollen on the physicochemical and in vitro properties of poly(acrylic acid) (PAA) hydrogel composites enriched with hydroxyapatite and modified with bee pollen as a prospective material for biomedical application with beneficial features including good osseointegration and anti-inflammatory effect. The phase and chemical composition of hydroxyapatite synthesized by wet-precipitation method was confirmed by means of X-ray diffraction (XRD) and Fourier Transform Infrared Spectroscopy (FT-IR). Proposed materials were investigated towards in vitro properties by immersion in the incubation fluids including artificial saliva, Ringer's solution and distilled water. The composites swelling ability was determined. Additionally, the chemical structure of the polymer matrix composites was confirmed by FT-IR method. Moreover, to characterize composite degradation process during 21-day incubation the FT-IR technique was used. In order to describe bee pollen feature, both scanning electron microscopy and X-ray fluorescence spectrometry were used. Presented research revealed that hydroxyapatite, as well as PAA undergo biodegradation during in vitro test. Moreover, matrices degradation results in incubation fluids pH decrease associated with anionic nature of PAA which is further enhanced by bee pollen release. The strongest pH drop effect was observed for Ringer's solution. Increase in conductivity of distilled water confirmed composites degradation process.

Keywords: *hydrogel, hydroxyapatite, bee pollen, composite, biomaterial*

[Engineering of Biomaterials 144 (2018) 8-14]

Introduction

In recent years hydrogels, due to their biocompatibility, cell-controlled degradability, and intrinsic cellular interaction have become one of the most important groups of materials used in medicine. Nowadays, hydrogels play an important role in dynamically developing field of tissue engineering where they are used as three-dimensional porous scaffolds to guide the growth of new tissues, as implantable materials in cartilage wound healing, drug delivery systems, wound dressings and in bone regeneration [1-6]. The structure and functions of those polymeric materials can be modified in a precisely controlled way. To foster new tissue formation hydrogels must meet a number of criteria that include physico-chemical (e.g. degradation and mechanics) and biological (e.g. cell adhesion) guidelines [7]. Hydrogels are made from natural polymers (e.g. collagen, chitosan, keratin) as well as synthetic polymers (e.g. poly(vinyl alcohol), PVA, poly(ethylene glycol), PEG, poly(acrylic acid), PAA). [8-15].

PAA has been intensively examined by many scientists in the context of biomedical applications, due to its biocompatibility, pH-sensitivity, solubility in water and aqueous solutions of inorganic salts and simultaneous lack of solubility in most organic liquids [16-17]. In neutral and alkaline solution acidic carboxyl groups of PAA are ionized and this leads to electrostatic repulsion of the polymer chains [18-19]. Over recent years, various PAA-based materials for the use in tissue engineering have been proposed [20].

Nowadays, polymeric hydrogels are mainly combined with different type of nancompounds (e.g. graphene oxide, carbon nanotubes, gold-silica nanoshells, nano-hydroxyapatite, ultra-high-molecular-weight polyethylene nanofibres) [21-25], biologically active proteins or peptides [26-27], and reinforced with inherently biocompatible particles (e.g. hydroxyapatite - HAp) [28-30].

HAp is the inorganic component of bones and teeth affecting their hardness and strength. HAp due to its porosity, bioactivity, biocompatibility and ability to form a good connection with the living tissues is willingly used as a component of different types of biomaterials, especially in dental and orthopaedic surgery as a filling material for biocompatible matrix [30-33].

In this research paper, we describe in detail the preparation, characterization and biocompatibility studies of three-dimensional hydrogel composite material prepared from acrylic acid, particles of HAp and agar (as a stabilizing agent), cross-linked by poly(ethylene glycol) diacrylate (*PEGDA*) under microwave irradiation and modified by different amounts of bee pollen. Experimental pharmacological studies performed on bee pollen confirmed its prospective application in hyper-lipidemia and atherosclerosis treatment as well as detoxification activity against organic solvents such as carbon tetrachloride and trichlorethylene [34-35]. Moreover, it is proved that bee pollen can be applied in the early old age symptoms and neurasthenic inertia treatment [36]. Pollen also shows high anti-inflammatory effect comparable to naproxen and indomethacin. Its anti-inflammatory effect is about inhibiting the activity of enzymes responsible for turning arachidonic acid into toxic compounds that induce inflammatory conditions in tissues [37]. Bee pollen containing hydrogel materials were presented in [38]; however hydroxyapatite addition in such materials can enhance their functionality by promoting osseointegration.

Materials and Methods

Materials

In experiments, all the reagents were of analytical grade and used without further purification. The chemicals: calcium oxide (CaO, to prepare aqueous solution of calcium hydroxide), 85% phosphoric acid (H_3PO_4), 25% ammonia solution, acrylic acid (AA), potassium hydroxide (KOH) and ammonium persulfate (APS) were purchased from POCh Gliwice, Poland. PAA was derived from Merck and agar was acquired from Sigma Aldrich.

Synthesis of hydroxyapatite

Hydroxyapatite was obtained by widely used synthesis technique called chemical or wet precipitation, based on the chemical reaction between calcium hydroxide $Ca(OH)_2$ (0.5M) and phosphoric acid H_3PO_4 (0.3M) in the presence of ammonia solution, according to the equation (1).

$$6H_3PO_4 + 10Ca(OH)_2 \xrightarrow{pH\approx 8} Ca_{10}(PO_4)_6(OH)_2 + 18H_2O \quad (1)$$

Preparation of PAA/HAp bee pollen modified hydrogel

Synthesis of PAA/HAp hydrogel was conducted in accordance with the procedure: 45 cm^3 of acrylic acid was neutralized with 50 cm^3 potassium hydroxide aqueous solution (40wt.%) and cooled slowly down to 30°C. After that 1 wt.% initiator (APS), 1wt.% crosslinking agent (*PEGDA*) and 20 g of stabilizing agent (agar) were added. Consequently, the obtained solution was finally mixed with previously prepared powder mixtures with various content of hydroxyapatite and ground bee pollen (TABLE 1). The resulting mixtures of powders and PAA, with other additions, were cross-linked by microwave irradiation at 600 W for 1 min, which resulted in formation of three-dimensional porous hydrogel structures.

Hydrogel swelling characteristics

1.0 g hydrogel samples were prepared in order to determine the swelling ratio of materials in simulated body fluid solution (TABLE 2), Ringer's solution (TABLE 3), artificial saliva (TABLE 4) and distilled water after twenty-three days of incubation at 37°C. The swelling ratio (X) was calculated according to the equation:

$$X = \frac{m - m_0}{m_0} \quad (2)$$

where m_o is the weight of hydrogel sample before incubation and m is its weight after incubation time.

Measurements of the ionic conductivity and pH value

Measurements of ionic conductivity and pH values of SBF, Ringer's solution, artificial saliva and distilled water were carried out during the hydrogels samples incubation in the mentioned fluids. The pH values changes were measured using Elmetron CP-401 waterproof pH Meter equipped with ERH – 111 composite electrode, and the ionic conductivity of solutions was investigated using Elmetron EC- 60 conductivity meter.

X-ray diffraction

The X-ray diffraction method was used to identify the hydroxyapatite particles in powder mixtures used to prepare hydrogel materials and phase identification of bee pollen. Analysis was performed using Philips X`Pert X-ray diffractometer equipped with a graphite monochromator PW 1752/00 with Ni filter (40 kV and 30 mA). All XRD patterns were recorded in the 2Θ range 10° – 60°.

IR Spectroscopy

The FT-IR studies, by KBr pellet technique, were utilized to determine the changes in the composition of the hydrogels after incubation time in comparison to their initial chemical composition using a Scimitar Series FTS 2000 Digilab spectrophotometer in the middle infrared range of 4000-400 cm^{-1}.

X-ray fluorescence spectrometry

In this paper XRF technique was used to analyze the chemical composition of bee pollen. The investigations were performed using Mini Pal PW 4025/00 X -ray PANalytical spectrometer with a sample changer, built-in helium system and analytical area of Na - U. Spectrometer was equipped with a semiconductor Si-PIN detector and X-ray lamp with a side window (9W) with Rh cathode.

TABLE 1. The composition of the powders used in synthesis.

Sample	HAp content [g]	Bee pollen content [g]
s1 1	4.0	2.0
s1 2	4.0	2.5
s1 3	4.0	3.0
s1 4	4.0	3.5
s1 5	4.0	4.0
s2 1	1.0	2.5
s2 2	1.0	3.5
s2 3	1.0	4.5
s2 4	1.0	5.5
s2 5	1.0	6.5

TABLE 2. The composition of the SBF solution.

Component	Concentration [g/L]
NaCl	8.035
$NaHCO_3$	0.355
KCl	0.225
$K_2HPO_4 \cdot 3H_2O$	0.231
$MgCl_2 \cdot 6H_2O$	0.311
HCl (1M)	39 ml
$CaCl_2$	0.292
Na_2SO_4	0.072
Tris	6.118
HCl (1M)	0-5 ml

TABLE 3. The composition of the Ringer's solution prepared according to [39].

Component	Ions content [mM/dm^3]
Na^+	147.0
K^+	4.0
Ca^{2+}	3.0
Cl^-	157.0

TABLE 4. The chemical composition of the artificial saliva prepared according to [40].

Component	Concentration [g/dm^3]
NaCl	0.400
KCl	0.400
$CaCl_2 \cdot H_2O$	0.765
$NaHPO_4 \cdot H_2O$	0.780
$Na_2S \cdot H_2O$	0.005
$(NH_2)_2CO_3$	1.000

Result and Discussion

SEM images of raw bee pollen at different magnifications are shown in FIG. 1. As it can be observed, bee pollen particles reveal elliptical shape and very uniform size distribution. Grains uniformity in size and shape is caused by gathering of bee pollen of the same plant species. In FIG. 1b it is shown that bee pollen particles reveal well-ordered porous distribution on their surface, which may result in significant improvement in adhesion to acrylic hydrogel matrix.

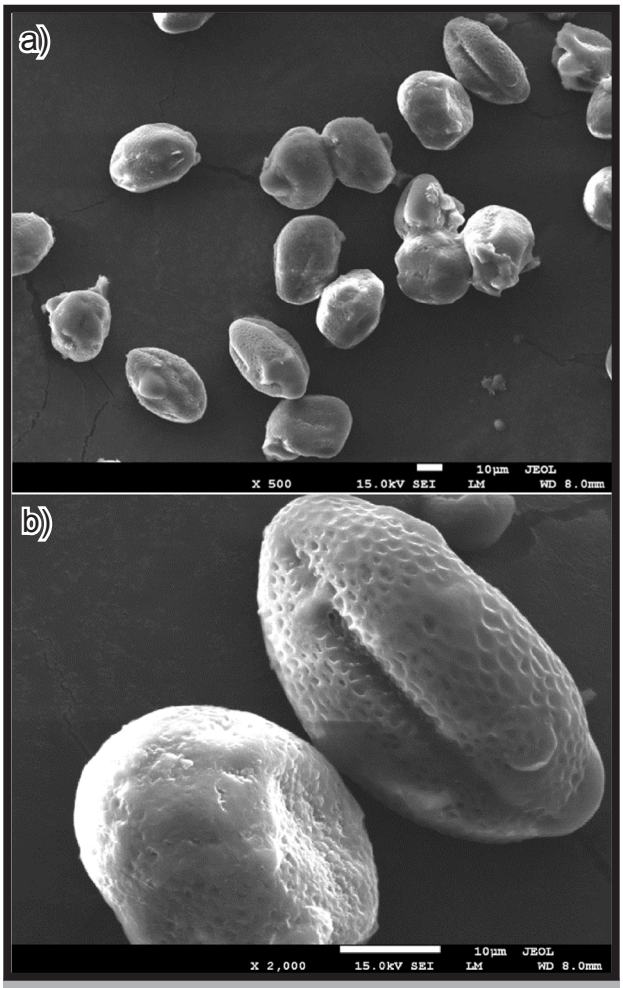

FIG. 1. SEM images of bee pollen at 500x magnification (a), and single particles of bee pollen at 2000x mgnification (b).

The analysis of bee pollen chemical composition was carried out with X-ray fluorescence technique. XRF studies (FIG. 2) have shown that potassium and calcium are the most abundant elements in the pollen tested. There is a noticeable difference between content of K and Ca and the content of the remaining elements in tested sample. In addition, sulfur, phosphorus, iron, copper and zinc were also detected in smaller amounts as compared to the previously discussed elements. The content of other elements such as manganese and silicon is negligible. What is important and worth mentioning is that the bee pollen chemical composition differs from their counterparts in different parts of the world. Therefore, the currently occurring season, plant species and climatic zone have a significant impact on the chemical composition of bee pollen.

X-ray diffraction patterns of hydroxyapatite and HA/bee pollen powder mixtures used in composites syntheses are shown in FIG. 3. The XRD pattern found in FIG. 3a is typical for crystalline monophasic hydroxyapatite. FIG. 3e shows XRD pattern of a raw bee pollen. The presence of pollen in the analyzed samples caused increase in the intensity of the background of pattern 1 b to 1 d in angular range 10° - 30°.

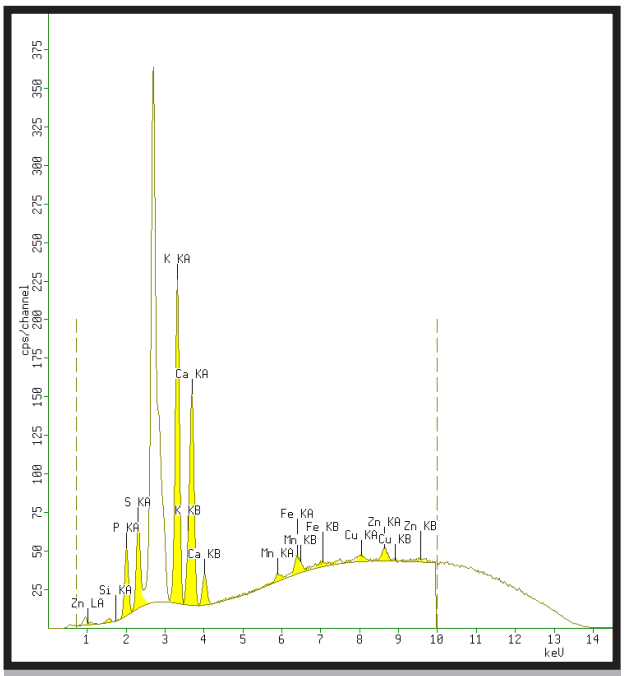

FIG. 2. X-ray fluorescence analysis of raw bee pollen.

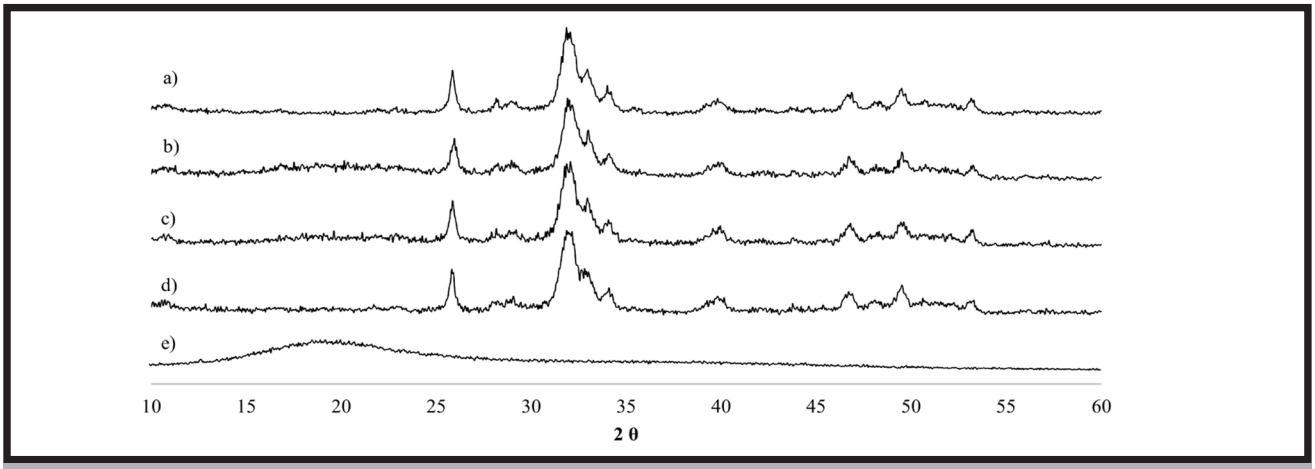

FIG. 3. XRD pattern of synthetic hydroxyapatite (a), S2 5 (b), S1 5 (c), S1 1 (d) and raw bee pollen (e).

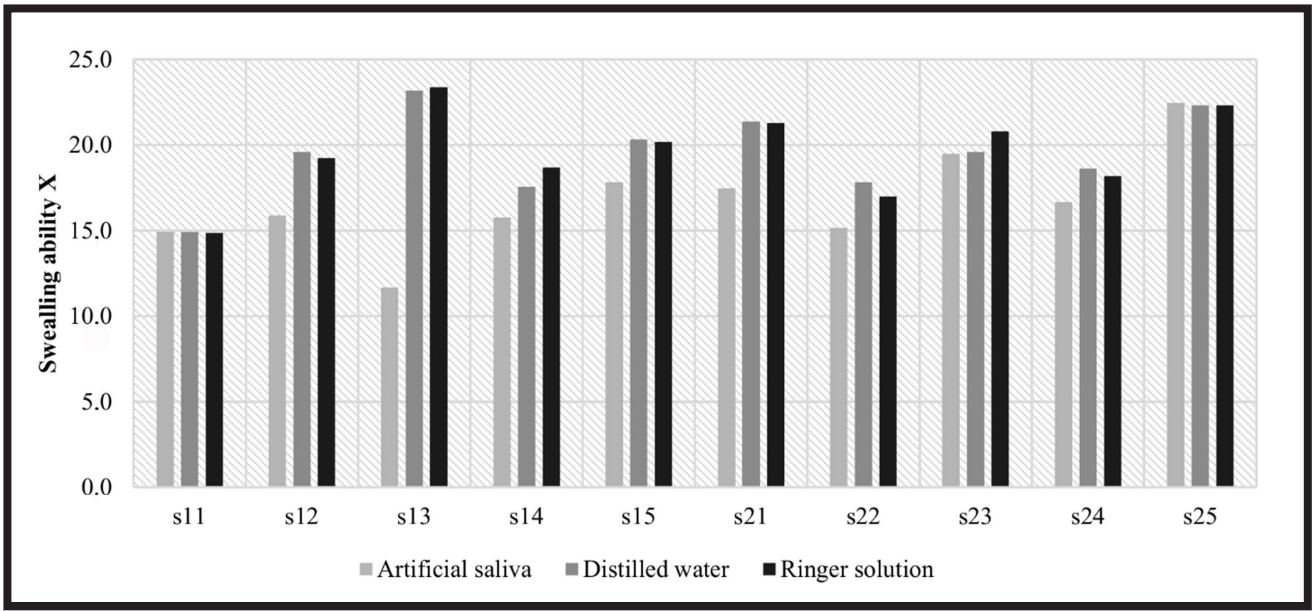

FIG. 4. Swealing ability of hydrogel composites.

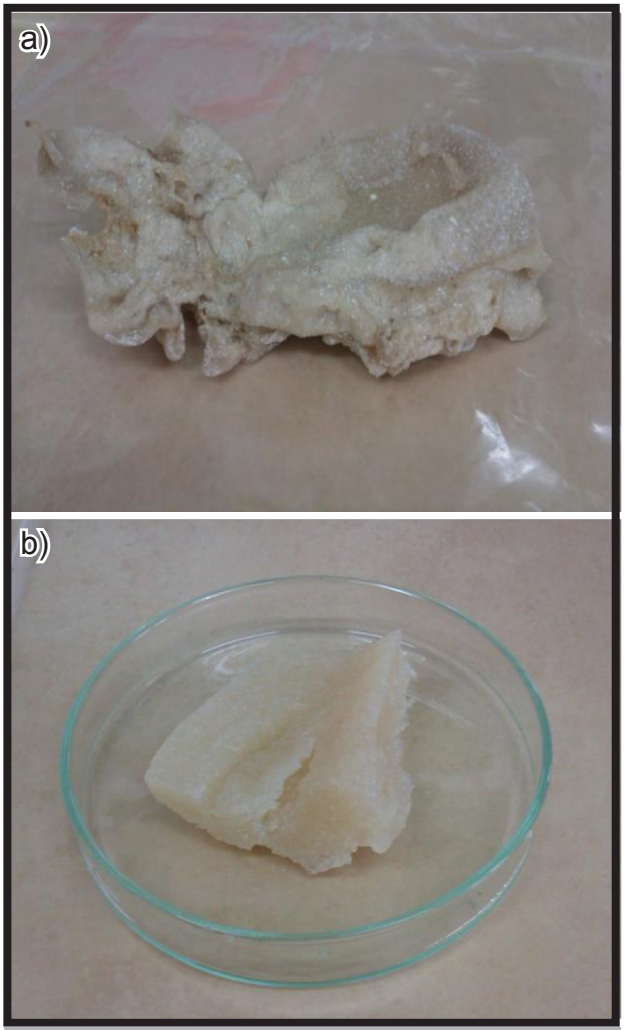

FIG. 5. Hydrogel composite before incubation (a) and after 21 days immersion in distilled water (b).

FIG. 4 shows swelling ability (X) of hydrogel composite materials incubated for 21 days in artificial saliva, distilled water and Ringer's solution. Measurement of specimens mass was carried out immediately after incubation without samples drying and revealed mass increase for all hydrogels.

High swelling ability of hydrogels is well-known feature of this type of materials. However, when measuring the mass of hydrogels, the possible degradation of the matrix should also be taken into account. The highest weight gain was observed for composites incubated in distilled water and Ringer's solution, which is due to pH of this solution. FIG. 5 shows hydrogel composites before incubation and after 21-day immersion in distilled water.

PAA is classified as a pH sensitive polymer which is caused by hydrophilic groups –COOH in polymer structure. At low pH, the interaction between the non-ionized carboxyl groups causes attraction of polymer segments, resulting in the shrinking of the macromolecule to compact form. With the increase in environmental pH, the carboxyl groups are ionized and repelled, causing the polymer chain expanding and water binding. At a pH < 4, the PAA is in a non-dissociated form, but at a pH > 8 the chain is fully ionized.

The pH changes of incubation fluids during samples immersion are associated with the presence of bioactive hydroxyapatite particles and biodegradable matrix, as well as releasing of bee pollen from the polymer matrix (FIG. 6). The changes in pH were more pronounced, the greater bee pollen/hydroxyapatite mass ratio was used for the composites synthesis, which confirms acidic nature of bee pollen. PAA, due to its anionic nature, also affected the pH drop. Changes in pH in individual solutions were not significant. The largest decrease in pH from 11.01 to 8.46 was recorded for the Ringer's solution.

FIG. 7 presents changes in the ionic conductivity of distilled water around the tested samples as a function of time. As a result, continuous growth of ionic conductivity was observed, along with an increase in the incubation time of composites in distilled water, although the rate and range of growth were varied. The different growth rate of ionic conductivity was due to different composition of composites. Composites with a medium and low content of bee pollen, for which both pH and conductivity were less pronounced, were more chemically stable.

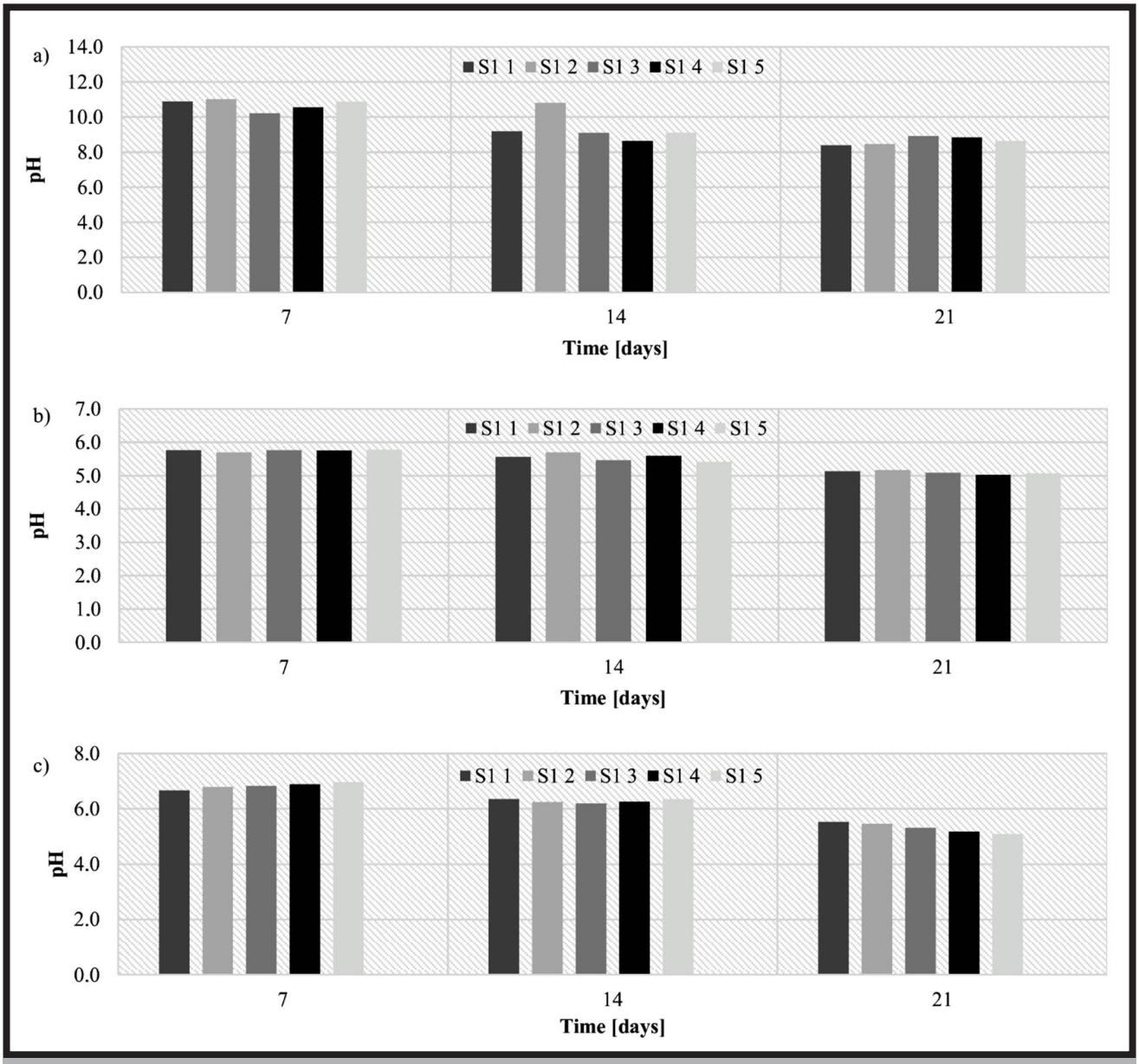

FIG. 6. The pH changes of Ringer's solution (a), artificial saliva (b) and distilled water (c).

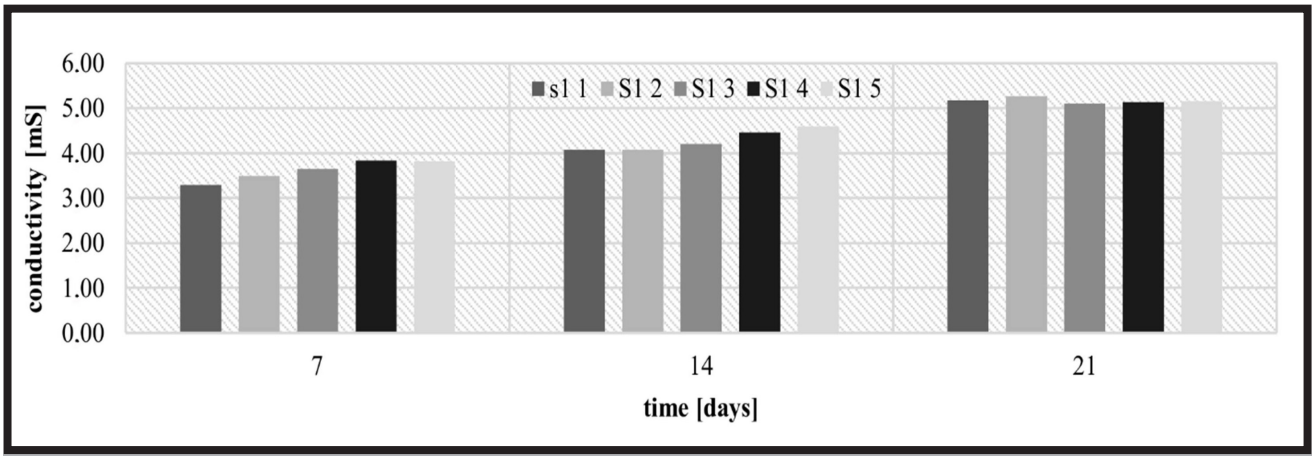

FIG. 7. Changes in conductivity of water during incubation s1 samples series.

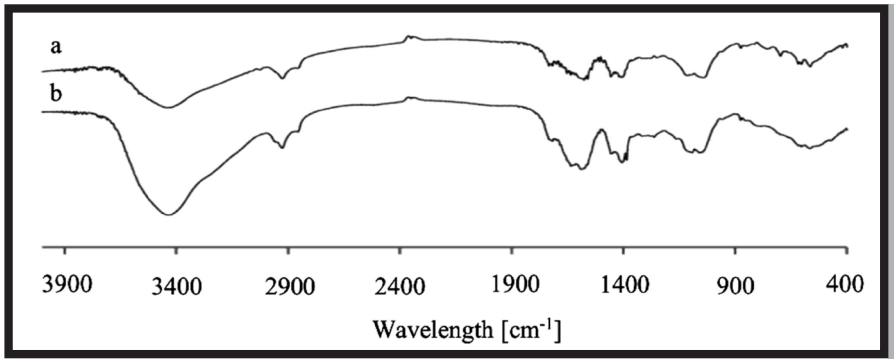

FIG. 8. FT-IR spectra of S2 5 (a) and S1 1 (b) samples before incubation.

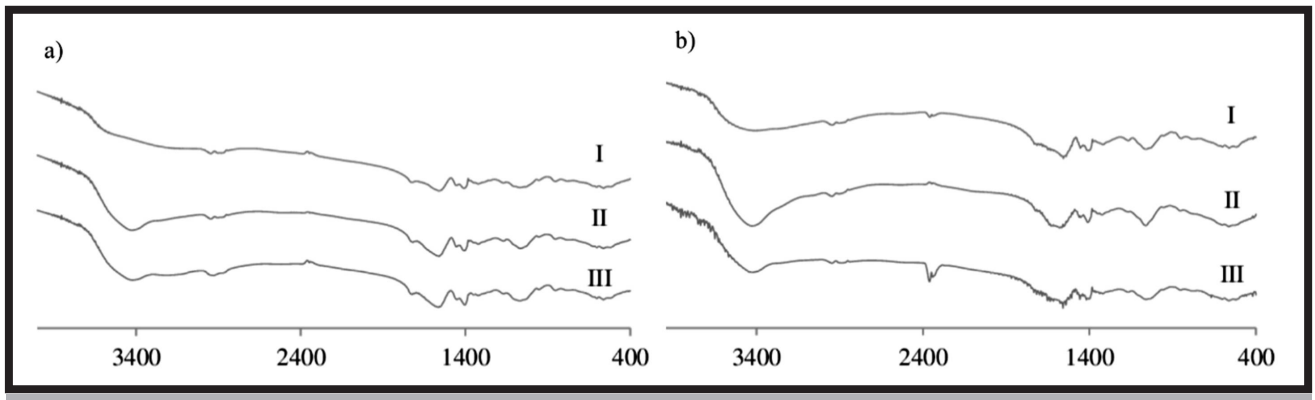

FIG. 9. FT-IR spectra of S2 5 (a) and S1 1 (b) samples after incubation in Ringer's solution (I), artificial saliva (II) and distilled water (III).

TABLE 5. IR band assignment of the samples.

Transmittance bands [cm^{-1}]	Peak assignment
560-600	bending vibration of PO_4^{3-} (O–P–O)
690, 740	in-plane deformation bending mode of CO_3^{2-} (O–C–O)
870	bending mode of CO_3^{2-} (A-type)
1030	triply degenerate asymmetric stretching mode of PO_4^{3-} (P–O)
1100	bending mode of PO_4^{3-} (P–O)
1375	symmetric bending deformation of C–H
1450	symmetrical scissor mode vibrations of the $–CH_2–$
1487	stretching mode of CO_3^{2-}
1550	vibrations of C=O
1715	ester groups stretching C=O
2785	symmetric stretching of $–CH_2–$
2962	asymmetric stretching of $–CH_2–$
3450	stretching mode of O–H

In order to fully characterize the HA-incorporated polymer matrix composites, FT-IR spectroscopy was employed. The FT-IR spectra of the chosen materials before immersion in incubation fluids are shown in FIG. 8.

FIG. 9 shows the FT-IR spectra after incubation in artificial saliva, distilled water and Ringer's solution. These spectra exhibit the presence of all bands that are found in HA specimen and pure PAA with intensity dependent on the content of the individual components of materials. Moreover, based on the FR-IR spectra, any interactions between materials ingredients that can lead to new chemical compounds formation are not observed thus PAA/HA/bee pollen composite materials may be considered as a mixture of this ingredients. FIG. 9a and 9b show the FT-IR spectra of specimens after 21-day incubation.

The degradation rate of materials is slightly dependent on the proportion of HA and bee pollen in the composite and a significant decrease in band intensity is observed after 21 days of immersion for all materials, indicating that both PAA and HA undergo degradation process in the incubation fluids. Transmittance bands revealed in the FT-IR spectra are assigned and summarized in TABLE 5.

Conclusions

The aims of this research were, firstly, to prepare hydrogel matrices made of PAA containing hydroxyapatite and modified with bee pollen and, secondly, to evaluate their prospective application in the field of biomedicine. Synthesis proposed in this paper allows to obtain 3D hydrogels enriched with bioactive phosphate and bee pollen that is recognized to be antiseptic and anti-inflammatory agent. Prepared composite materials present good sorption capacity against different fluids used in biomedical testing, such as Ringer's solution and artificial saliva. In vitro tests performed in this research proved that the investigated materials are stable in body-simulated conditions during 21 days of incubation. Given the fact that acrylic hydrogels are already applied as wound dressing materials, further investigations should be focused on adoption this structure in the field of biomaterials supporting bone regeneration, which can be achieved by bioactive phosphates incorporation. It can be presumed that such modified hydrogels would possess beneficial properties and would support osseointegration.

Acknowledgments

The authors gratefully acknowledge financial support from National Science Centre in the frame of UMO-2016/21/D/ST8/01697.

References

[1] Dhandayuthapani B., Yoshida Y., Maekawa T., Kumar D.S.: Polymeric Scaffolds in Tissue Engineering Application: A Review. International Journal of Polymer Science 2011 (2011) 1-19.
[2] Wu M., Bao B., Yoshii F., Makuuchi K.: Irradiation of Crosslinked, Poly(Vinyl Alcohol) Blended Hydrogel for Wound Dressing. Journal of Radioanalytical and Nuclear Chemistry 250 (2001) 391-395.
[3] Bakó J., Vecsernyés M., Ujhelyi Z., Kovácsné I.B., Borbíró I., Bíró T., Borbély J., Hegedűs C.: Composition and characterization of in situ usable light cured dental drug delivery hydrogel system. Journal of Materials Science: Materials in Medicine 24 (2013) 659-666.
[4] Wang Q.Q., Kong M., An Y., Liu Y., Li J.J., Zhou X., Feng C., Li J., Jiang S.Y., Cheng X.J.: Hydroxybutyl chitosan thermo-sensitive hydrogel: a potential drug delivery system. Journal of Materials Science 48 (2013) 5614-5623.
[5] Huang K.T., Huang C.J.: 1st Global Conference on Biomedical Engineering & 9th Asian-Pacific Conference on Medical and Biological Engineering IFMBE Proceedings 47:35 (2015)
[6] Smith T.J., Kennedy J.E.: Rheological and thermal characteristics of a two phase hydrogel system for potential wound healing application. Journal of Materials Science 45 (2010) 2884-2891.
[7] Pietrucha K., Verne S.: Synthesis and Characterization of a New Generation of Hydrogels for Biomedical Applications. World Congress on Medical Physics and Biomedical Engineering Munich, Germany (2009) 1-4.
[8] Schmedlen R.H., Masters K.S., West J.L.: Photocrosslinkable polyvinyl alcohol hydrogels that can be modified with cell adhesion peptides for use in tissue engineering. Biomaterials 23 (2002) 4325-4332.
[9] Du H., Liu M., Yang X., Zhai G.: The design of pH-sensitive chitosan-based formulations for gastrointestinal delivery. Drug Discov Today 20 (2015) 1004-1011.
[10] Giri T.K., Thakur A., Alexander A., Ajazuddin, Badwaik H., Tripathi D.K.: Modified chitosan hydrogels as drug delivery and tissue engineering systems: present status and applications. Acta Pharmaceutica Sinica B 2 5 (2012) 439-449.
[11] Hong Z., Song Y., Gong Y., Mao Z., Gao C., Shen J.: Covalently crosslinked chitosan hydrogel: Properties of in vitro degradation and chondrocyte encapsulation. Acta Biomaterialia 3 (2007) 23-31.
[12] Tseng H., Puperi D.S., Kim E.J., Ayoub S., Shah J.V., Cuchiara M.L., West J.L., Grande-Allen K.J.: Anisotropic poly (ethylene glycol)/polycaprolactone hydrogel-fiber composites for heart valve tissue engineering 20 (2014) 2634-2645.
[13] Parlato M., Reichert S., Barney N., Murphy W.L.: Poly(ethylene glycol) hydrogels with adaptable mechanical and degradation properties for use in biomedical applications. Macromolecular Bioscience 14 (2014) 687-698.
[14] Nakata R., Tachibana A., Tanabe T.: Preparation of keratin hydrogel/hydroxyapatite composite and its evaluation as a controlled drug release carrier. Materials Science and Engineering: C 41 (2014) 59-64.
[15] Nho Y.C., Park J.S., Lim Y.M.: Preparation of Poly(acrylic acid) Hydrogel by Radiation Crosslinking and Its Application for Mucoadhesives. Polymers 6 (2014) 890-898.
[16] Ahn J.S., Choi H.K., Cho C.S.: A novel mucoadhesive polymer prepared by template polymerization of acrylic acid in the presence of chitosan. Biomaterials 22 (2001) 923-928.
[17] Hu H., Wang H., Du Q.: Preparation of pH-sensitive polyacrylic acid hollow microspheres and their release properties. Soft Matter 8 (2012) 6816-6822.
[18] Almeida H., Amaral M.H., Lobão P.: Temperature and pH stimuli-responsive polymers and their applications in controlled and selfregulated drug delivery. Journal of Applied Pharmaceutical Science 02 (2012) 1-10.
[19] Bajpai A.K., Shukla S.K., Bhanu S., Kankane S.: Responsive polymers in controlled drug delivery. Progress in Polymer Science 33 (2008) 1088-1118.
[20] Mohammad Z.M., Kourosh K.: Superabsorbent Polymer Materials: A Review. Iranian Polymer Journal 17 (2008) 451-477.
[21] Kim D., Lee E., Lee H.S., Yoon Y.: Energy efficient glazing for adaptive solar control fabricated with photothermotropic hydrogels containing graphene oxide. Scientific Reports – Nature 5 (2015) 7646.
[22] Yang Z., Cao Z., Sun H., Li Y.: Composite Films Based on Aligned Carbon Nanotube Arrays and a Poly(N-Isopropyl Acrylamide) Hydrogel. Advanced Materials 20 (2008) 2201-2205.
[23] Strong L.E., Dahotre S.N., West J.L.: Hydrogel-nanoparticle composites for optically modulated cancer therapeutic delivery. Journal of Controlled Release 178 (2014) 63-68.
[24] Fu S., Ni P., Wang B., Chu B., Zheng L., Luo F., Luo J., Qian Z.: Injectable and Thermo-Sensitive PEG-PCL-PEG Copolymer/collagen/n-HA Hydrogel Composite for Guided Bone Regeneration. Biomaterials 33 (2012) 4801-4809.
[25] Holloway J.L., Lowman A.M., VanLandingham M.R., Palmese G.R.: Interfacial optimization of fiber-reinforced hydrogel composites for soft fibrous tissue applications. Acta Biomaterialia 10 (2014) 3581-3589.
[26] Golas P.L., Matyjaszewski K.: Marrying click chemistry with polymerization: expanding the scope of polymeric materials. Chemical Society Reviews 39 (2010) 1338-1354.
[27] Kopeček J.: Hydrogel biomaterials: a smart future? Biomaterials 28 (2007) 5185-5192.
[28] Kutikov A.B., Skelly J.D., Ayers D.C., Song J.: Templated repair of long bone defects in rats with bioactive spiral-wrapped electrospun amphiphilic polymer/hydroxyapatite scaffolds. ACS Applied Materials & Interfaces 7 (2015) 4890-4901.
[29] Turco G., Marsich E., Bellomo F., Semeraro S., Donati I., Brun F., Grandolfo M., Accardo A., Paoletti S.: Alginate/Hydroxyapatite Biocomposite For Bone Ingrowth: A Trabecular Structure With High And Isotropic Connectivity. Biomacromolecules 10 (2009) 1575-1583.
[30] Li Z., Su Y., Xie B., Wang H., Wen T., He C., Shen H., Wu D., Wang D.: A tough hydrogel–hydroxyapatite bone-like composite fabricated in situ by the electrophoresis approach. Journal of Materials Chemistry B 1 (2013) 1755-1764.
[31] Kikuchi M., Ikoma T., Itoh S., Matsumoto H.N., Koyama Y., Takakuda K., Shinomiya K., Tanaka J.: Biomimetic synthesis of bone-like nanocomposites using the self-organization mechanism of hydroxyapatite and collagen. Composites Science and Technology 64 (2004) 819-825.
[32] Kobayashi H., Kato M., Taguchi T., Ikoma T., Miyashita H., Shimmura S., Tsubota K. Tanaka J.: Collagen immobilized PVA hydrogel-hydroxyapatite composites prepared by kneading methods as a material for peripheral cuff of artificial cornea. Materials Science and Engineering: C 24 (2004) 729-735.
[33] Wu G., Su B., Zhang W., Wang C.: In vitro behaviors of hydroxyapatite reinforced polyvinyl alcohol hydrogel composite. Materials Chemistry and Physics 107 (2008) 364-369.
[34] Pola M., Okoń K., Przybyło R., Frasik W.: Cardioprotective properties of hydrophilic pollen extract (HPE). Journal of Pathology 49 (1998) 109-112.
[35] Asafova N., Orlov B., Kozin R.: Physiologically Active Bee Products (2001)
[36] Pascoal A., Rodrigues S., Teixeira A., et al.: Biological activities of commercial bee pollens: antimicrobial, antimutagenic, antioxidant and anti-inflammatory. Food and Chemical Toxicology 63 (2014) 233-239.
[37] Kokubo T., Kushitani H., Sakka S., Kitsugi T., Yamamuro T.: Solutions able to reproduce in vivo surface-structure changes in bioactive glass-ceramic A-W. Journal of Biomedical Materials Research 24 (1990) 721-734.
[38] Tyliszczak B., Walczyk D., Wilczyński S.: Acrylic hydrogels modified with bee pollen for biomedical applications. Journal of Applied Pharmaceutical Science 5 (2015) 010-014.
[39] Raynaund S., Champion E., Lafon J. P., Bernache – Assollant D.: Calcium phosphate apatites with variable Ca/P atomic ratio I. Synthesis, characterisation and thermal stability of powders. Biomaterials 23 (2002) 1065-1072.
[40] ISO 10271:2001

3D PRINTED POLY L-LACTIC ACID (PLLA) SCAFFOLDS FOR NASAL CARTILAGE ENGINEERING

Adam Jabłoński[1], Jerzy Kopeć[1], Samuel Jatteau[1,2], Magdalena Ziąbka[3], Izabella Rajzer[1]*

[1] ATH University of Bielsko-Biala,
Faculty of Mechanical Engineering and Computer Science,
Department of Mechanical Engineering Fundamentals,
ul. Willowa 2, 43-309 Bielsko-Biała, Poland
[2] University of Lorraine, Polytech Nancy,
2 rue Jean Lamour, 2 rue Jean Lamour,
54519 Vandoeuvre les Nancy Cedex, Nancy, France
[3] AGH University of Science and Technology,
Faculty of Materials Science and Ceramics,
Department of Ceramics and Refractories,
Al. Mickiewicza 30, 30-059 Krakow, Poland
*e-mail: irajzer@ath.bielsko.pl

Abstract

In this study the scaffolds for nasal cartilages replacement were designed using a software called Rhino 3D v5.0. The software parameters considered for the design of scaffolds were chosen and the scaffolds were fabricated using Fused Deposition Modeling (FDM), a rapid prototyping technology, using poly(L-lactic acid) (PLLA) filament. The topographical properties of the scaffolds were calculated through 3D model simulation. The morphology of obtained scaffold was observed by Scanning Electron Microscopy (SEM). The biological properties, i.e. bioactivity of the scaffolds, were assessed in Simulated Body Fluid. On the basis of natural cartilages images the external shape of the scaffold was designed using the 3D modeling software.

The FDM is a useful method in fabrication of 3D bioactive implants for cartilage tissue engineering. Thanks to the use of 3D modeling software, it is possible to prepare and manufacture artificial cartilage in a controlled manner. Artificial scaffold made of PLLA polymeric matrix may mimic natural one by shape, topography, geometry, pore size, and their distribution. In addition, it is possible to guarantee appropriately selected biological properties such as biocompatibility and high bioactivity of scaffolds, which was proved using scanning electron microscopy (SEM) analysis. The surface observation of the 3D printed scaffolds showed in vitro formation of apatite after immersion in the SBF. What is more, it is possible to match the scaffold not only to the large cavity but also individually to each patient.

Keywords: *3D printing, PLLA, nasal cartilages, scaffolds, tissue engineering*

[Engineering of Biomaterials 144 (2018) 15-19]

Introduction

The damaged or lost nasal cartilage is an important problem for the patients and also for the laryngologist and plastic surgeons. Injured natural cartilage is slow and difficult to heal, and has almost no ability to regrow itself [1]. Untreated cartilage defects lead to degeneration of tissues. Even small chondral defects may necessitate surgical intervention. Therefore, it is necessary to find an appropriate cartilage scaffold that will be able to assist in tissue regeneration. Cartilage scaffold is typically made of porous biodegradable materials that provide the mechanical support during repair and regeneration of damaged or diseased cartilage. Scaffolding faces challenge in mimicking the structure of natural tissue. A high-level control over the architecture, mechanical properties and composition of the materials in contact with cells is really essential [2]. Scaffolds not only provide a structural support to the growing tissue, but also play key role as a construct in guiding tissue regeneration. The scaffolds are seeded with cells and growth factors in order to mimic the extracellular matrix and support tissue growth [3]. 3D printing is increasingly employed to manufacture scaffolds for tissue engineering applications [4-6]. Unlike conventional methods of making cellular scaffolds, three-dimensional (3D) printing or additive manufacturing opens up the new possibilities to fabricate those customizable intricate designs with highly interconnected pores [7]. The ability to use 3D medical imaging data from MRI and CT of patient data is important to provide the potential of repairing damaged or diseased tissues regions, and perhaps eventually the whole organs [8]. The CAD-based methods are the most widely used in this field [9]. Rapid Prototyping (RP) involves computer-aided design (CAD) and manufacturing (CAM). The use of a three dimensional CAD model in RP enables to create a complex 3D geometries that are limited only by the resolution of the equipment. RP also allows the recreation of geometries by computed tomography (CT) scans, which enables the exact reproduction of natural tissues. The repertoire of RP techniques is broad, and includes among others selective laser sintering (SLS), stereolithography (SLA) and fused deposition modeling (FDM) [10-15].

In this work, fused deposition modeling (FDM) was used to fabricate scaffolds with controlled scaffold architecture, porosity as well as the shape of the resulted implants for nasal cartilages application. On the basis of natural cartilages images the external shape of the scaffold was designed using the 3D modeling software.

Materials and Methods

The main scaffold fabrication steps by Rapid Prototyping techniques are shown in FIG. 1. The fabrication process starts with a 3D design of the scaffold using CAD software, afterwards, the model is saved as -.STL file format and transferred to FDM printer, then the scaffold is directly fabricated layer by layer. The digital spatial model of scaffold prototype was obtained using 3D surface modeller (Rhino3D v5). The 3D model had lattice form with an additional reinforced frame (FIG. 2).

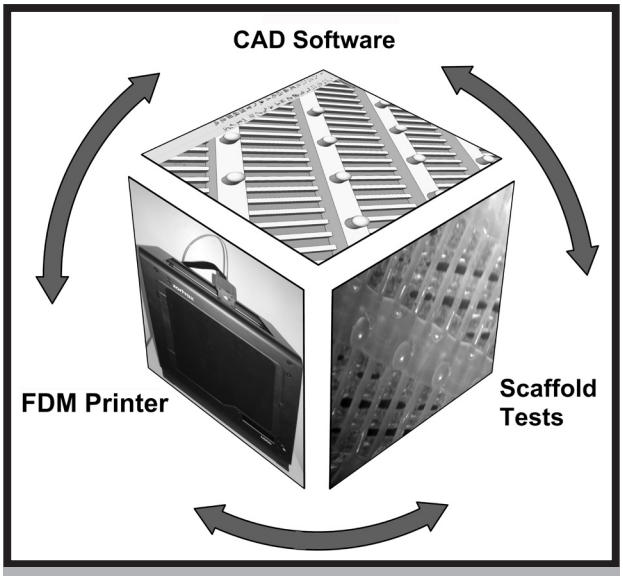

FIG. 1. Rapid prototyping of scaffolds with FDM.

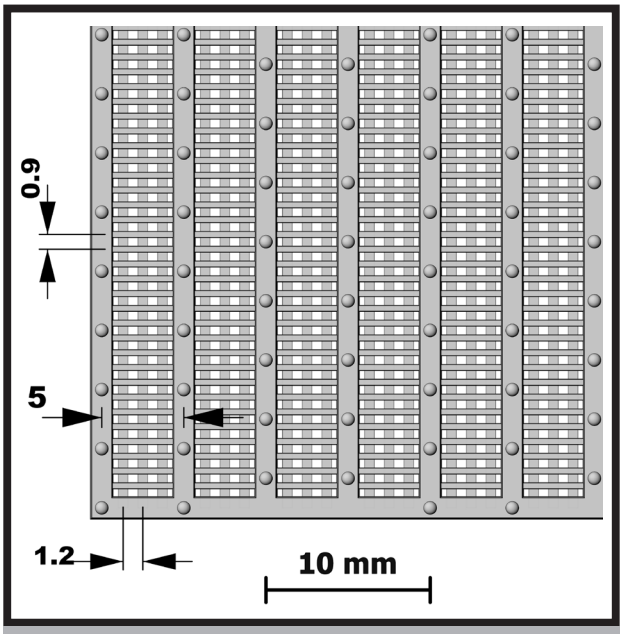

FIG. 2. Top view of the lattice microstructure of the designed scaffold (scaffold prototype).

The restraining frame parameters were: 1.4 mm width, 1.2 mm height, and spacing 5 mm. The filling bars were 0.4 mm wide and 0.4 mm high, and they were spaced at 0.9 mm intervals. The distance between filament strands (the shortest distance between two filaments located within the same layer) for the upper layer was 0.5 mm and for the bottom one was 0.6 mm. The dimensions of the scaffold were: length 46.4 mm, width 44.6 mm, height (thickness of the scaffold) 1.6 mm. To study the potential of scaffold topography, and its influence on future cell behaviour protruding posts were also designed. The posts diameter was 0.8 mm and their height was 0.9 mm. After modelling in CAD software the geometry properties of the scaffolds were calculated through 3D model simulation (i.e.: volume, porosity, total area, total edge length) (TABLE 1).

TABLE 1. The comparison of the topographical scaffold properties for lattice microstructure and solid cuboid.

Micro-structure	Volume [mm^3]	Porosity [%]	Total Area [mm^2]	Total Edge Length [mm]
Lattice structure	1278.1	61.4	6341.1	13780.1
Reference cuboid	3311.1	0.0	4430.1	370.4

Poly(L-lactic acid) (PLLA, 3D4Makers) with a diameter of 1.75 mm, molecular weight 60000 – 80000 Da, and viscosity of 300000 CP was used as filament for 3D printer (Zortrax M200, Poland). PLLA is a biodegradable polymer widely used in tissue engineering due to its biocompatibility and non-toxic degradation products. The extrusion-based RP technique, also known as Fused Deposition Modelling (FDM) was applied. A PLLA filament was fused and guided by an extrusion nozzle to form 3D scaffolds. Printer nozzle temperature was 210°C. The material left the extruder in a liquid form and solidified upon contact with the fabrication platform (temp. range: 20-60°C). The previously formed layer was the substrate for the next layer. A temperature was maintained just below the solidification point of the material to assure good interlayer adhesion.

The samples were evaluated with Stereomicroscope (SN from OPTA-TECH Company, equipped with CMOS 3 camera and OptaViewIS software) and with scanning electron microscope (Nova NanoSEM 200, FEI) equipped with EDS analysis. The samples were coated with carbon layer before observation.

To assess the biological properties of the obtained PLLA scaffolds, 1.5 x SBF (Simulated Body Fluid) solution with the ion concentration nearly 1.5 x as those in human blood plasma, was prepared following the Kokubo's recipe [16]. Printed scaffolds were exposed to UV light, each side of scaffold for 15 min. Four samples of PLLA scaffolds (10 x 10 mm squares) were immersed in 1.5 x SBF solution at 37°C for 1, 3 and 7 days respectively. The SBF solution was changed every 2 or 3 days in order to optimize the *in vitro* simulation. After each period of time samples were washed with deionized water, dried and observed with scanning electron microscope.

Results and Discussions

Using FDM - additive fabrication process it was possible to fabricate the PLLA scaffolds from a computer-aided design (CAD) file. The designed shape and porosity of the scaffolds as well as their microstructure were built using 3D drawing computer software -Rhino. It can be seen that the 3D model had lattice form with an additional reinforced frame (FIG. 2). The main features of selected pattern were: easy modelling, plenty of outer and inner surfaces that constitute places where the cells can grow (FIG. 3). The ability of cells to migrate in 3D environments under defined external cues (i.e. in the form of topography) in the host organism is essential for life [17]. Scaffold topography determine biological processes, such as cell migration and morphogenesis. Therefore it will be necessary in our further work to study the effect of designed microstructures on the cell behaviour. The additional small posts were added in scaffold design to study (at the later stage) cell behaviour on differently structured substrates and also in order to support the anchoring of the scaffold.

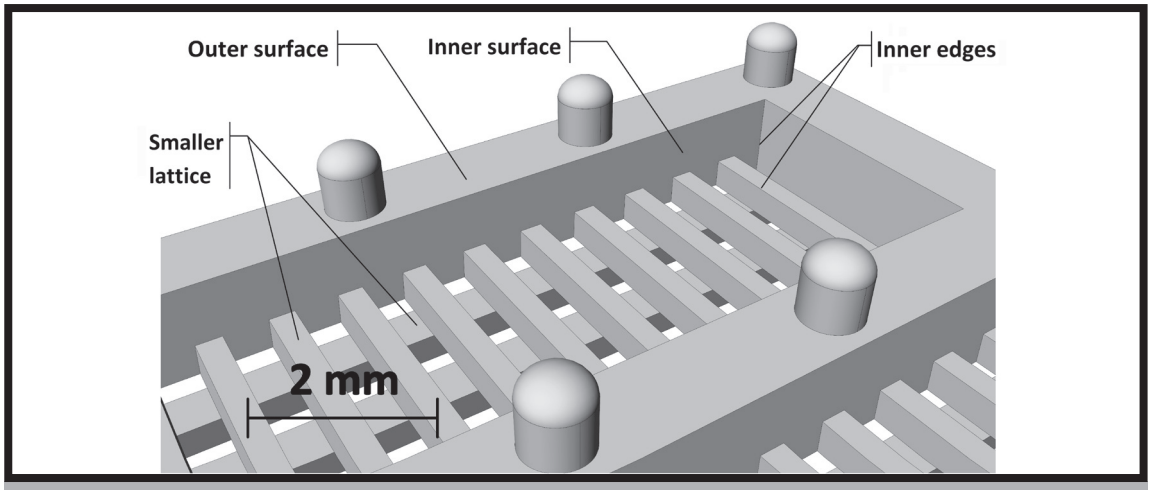

FIG. 3. Geometry of the 3D model of prototype scaffold.

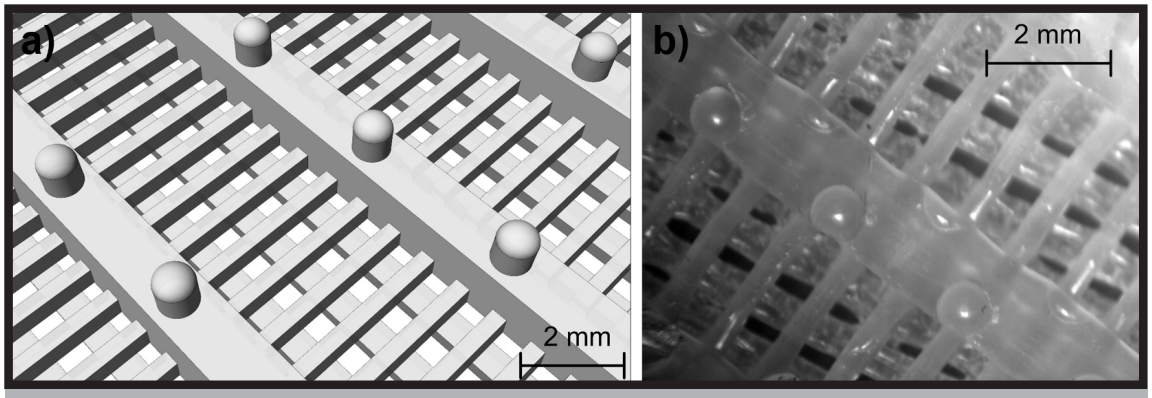

FIG. 4. View of the 3D model of scaffold (left) and printed microstructure (right).

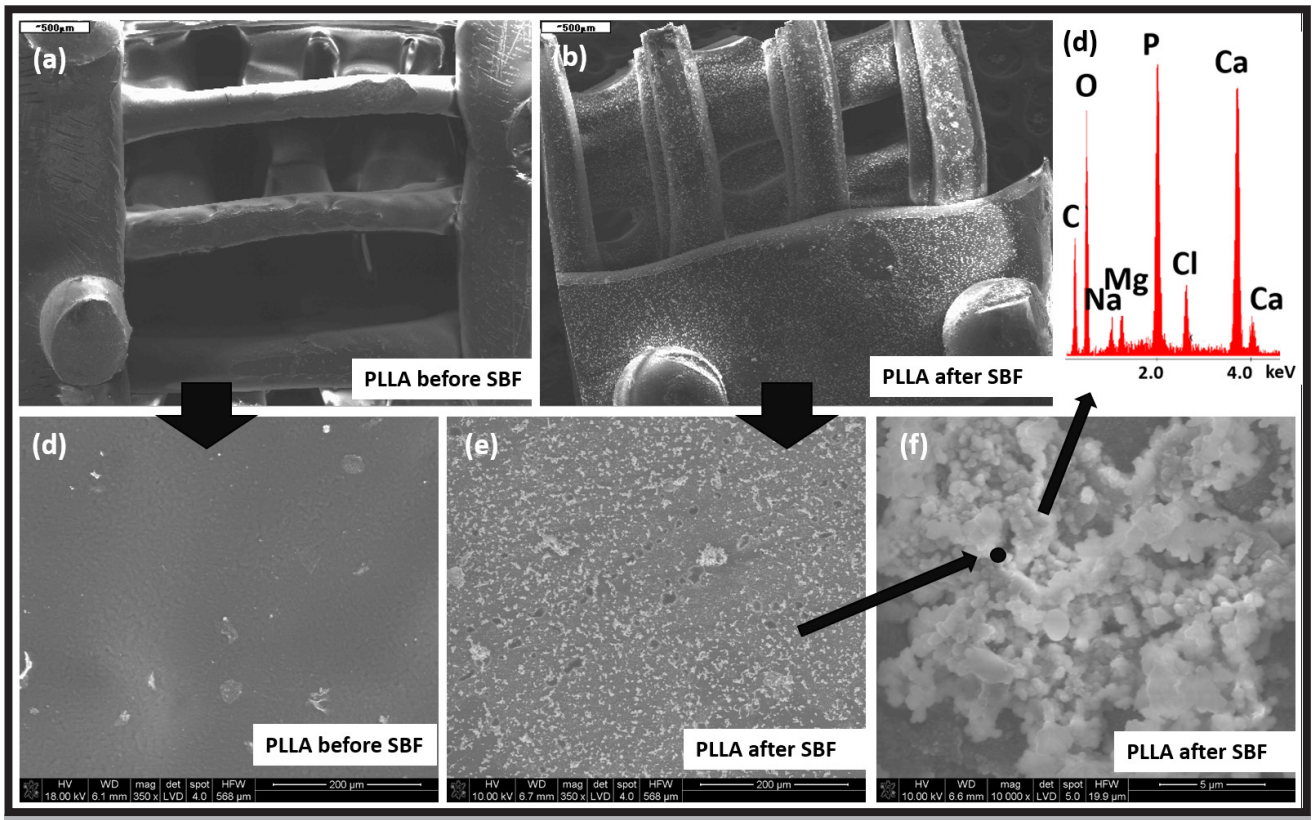

FIG. 5. SEM images of printed scaffolds before and after immersion in the physiological fluid (SBF) together with the EDS analysis.

The properties of the lattice microstructure of designed scaffold were compared with relevant one for solid cuboid (TABLE 1). The main advantages of proposed scaffold design are high porosity, around 60%, and high total length of edges (almost 14 meters). In this work we wanted to fabricate scaffolds with pores bigger than usually are used in scaffolds for cartilage application, in order to ensure the proper fixation of the scaffolds by the use of surgical curved needle during the implantation process. The solid model of the scaffold and its printed version are shown in FIG. 4. The diameter of the filament strands in the printed scaffolds were about 450 μm (upper layer) and 660 μm (bottom layer), determined from the stereoscopic microscope images (FIG. 4b.) and SEM images (FIG. 5a and d).

Formation of apatite was evaluated in Simulated Body Fluid (SBF). PLLA scaffolds can develop bone-like apatite after immersion in SBF without any additional modification with bioactive particles. The apatite formation mechanism for porous PLLA is related with the hydrolysis of PLLA, which result in a negatively charged PLLA surface [18]. The positively charged calcium ions in the SBF solution are attracted to the hydrolysed PLLA surface and apatite forms through the attraction of phosphate groups from the solution and the increase of local apatite ion activity product [19]. After 7 days of immersion in SBF solution, globular precipitates cover the surface of both (upper and bottom) layers of printed scaffolds (FIG. 5). The EDS analysis (FIG. 5d) reports the presence of calcium and phosphorus, what means that apatite layer was formed on 3D printed PLLA, proving its bioactivity.

The developments in FDM technologies imply the success of surgical operations where any part of the human body, e.g. nose, can be reconstructed by obtaining images from X-ray CT scans of the patients. In this study a nasal cartilage implant was designed on the basis of real cartilage images. The exemplary process of design is depicted in FIG. 6. At the beginning the shape similar to the biological structure was drawn and it was extruded. Second step was creating basic frame (so cold shelling method of solid modelling). The third step was applying formerly tested lattice structure as a filling and space where cells can grow (Boolean operations and tapered extrusion was chosen as a method of CAD modelling). Future experiments will be also undertaken in order to cover the obtained 3D printed scaffold with electrospun hydrogel nanofibers for better chondrocyte adhesion and proliferation.

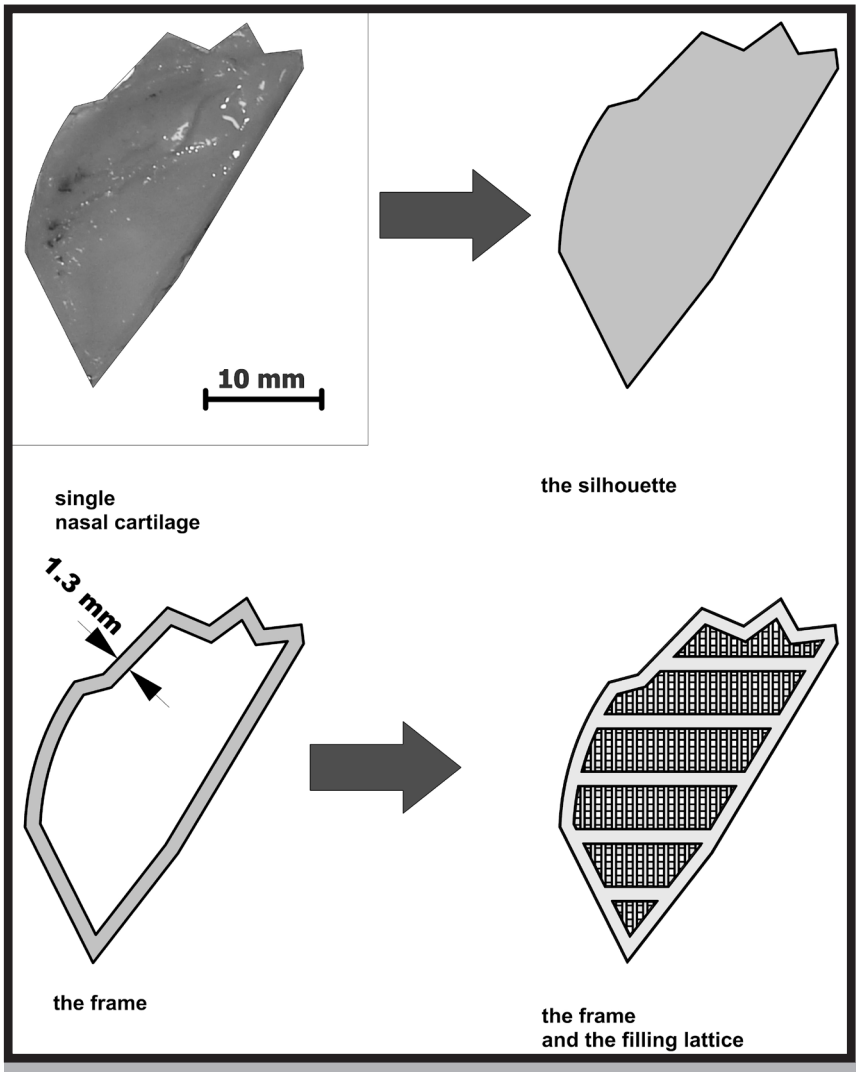

FIG. 6. Process of design nasal cartilage implant from natural cartilage image (CAD software involved).

Conclusions

Although it is difficult to fabricate the scaffold that fulfils all requirements for nasal cartilage implants, our preliminary research show the potential of using FDM method in fabrication of 3D bioactive implants for cartilage tissue engineering. It was possible to have control over the architecture of PLLA, allowing the manufacturing of microstructures with designed scaffolds shape, topography, geometry, pore size, and size distribution. On the basis of natural cartilages images the external shape of the scaffold was predesigned using the 3D modeling software. *In vitro* formation of apatite on the 3D printed scaffolds after immersion in SBF demonstrates scaffolds bioactivity.

Acknowledgments

This work was supported by the National Science Centre, Poland in the frame of project: "Layered scaffolds for nasal cartilages reconstruction fabricated by 3D printing and electrospinning" 2015/18/E/ST5/00189 (Sonata Bis 5). The authors would like to acknowledge Agnieszka Wiatr (form Coll Med, UJ The University Hospital in Cracow) for providing natural cartilage.

References

[1] C. Chung, J.A. Burdick: Engineering cartilage tissue. Advanced Drug Delivery Reviews 60 (2008) 243-262.
[2] K.K. Gómez-Lizárraga, C. Flores-Morales, M.L. Del Prado--Audelo, M.A. Álvarez-Pérez, M.C. Piña-Barba, C. Escobedo: Polycaprolactone- and polycaprolactone/ceramic-based 3D-bioplotted porous scaffolds for bone regeneration: A comparative study. Materials Science and Engineering C 79 (2017) 326-335.
[3] K. Haberstroh, et. al.: Bone repair by cell-seeded 3D-bioplotted composite scaffolds made of collagen treated tricalciumphosphate or tricalciumphosphate-chitosan-collagen hydrogel or PLGA in ovine critical-sized calvarial defects. J. Biomed. Mater. Res. B Appl. Biomater. 93 (2010) 520-530.
[4] B. Derby: Printing and prototyping of tissues and scaffolds. Science 338 (2012) 921-926.
[5] S. Yang, K.-F. Leong, Z. Du, C.-K. Chua: The design of scaffolds for use in tissue engineering. Part II. Rapid prototyping techniques. Tissue Eng. 8 (2002) 1-11.
[6] B.C. Gross, J.L. Erkal, S.Y. Lockwood, C. Chen, D.M. Spence: Evaluation of 3D Printing and Its Potential Impact on Biotechnology and the Chemical Sciences. Anal. Chem. 86 (7) (2014) 3240-3253.
[7] D. Dimitrov, K. Schreve, N. de Beer: Advances in Three Dimensional Printing - State of the Art and Future Perspectives. Rapid Prototyping Journal 12 (2006)136-147.
[8] F. Rengier, A. Mehndiratta, H. et al.: 3D printing based on imaging data: review of medical applications. Int. J. Comput. Assist. Radiol. Surg. 5 (2010) 335-341.
[9] S. Giannitelli, D. Accoto, M. Trombetta, A. Rainer: Current trends in the design of scaffolds for computer-aided tissue engineering. Acta Biomater. 10 (2) (2014) 580-594.
[10] D.W. Hutmacher, M. Sittinger, M.V. Risbud: Scaffold-based tissue engineering: rationale for computer-aided design and solid free--form fabrication systems. Trends Biotechnol. 22 (2004) 354-362.
[12] E. Sachs, M. Cima, J. Cornie: Three-dimensional printing: rapid tooling and prototypes directly from a CAD model, CIRP Ann. Manuf. Technol. 39 (1990) 201-204.
[13] R. Landers, R. Mülhaupt: Desktop manufacturing of complex objects, prototypes and biomedical scaffolds by means of computer--assisted design combined with computer- guided 3D plotting of polymers and reactive oligomers. Macromol. Mater. Eng.282 (2000) 17-21.
[15] F.P.W. Melchels, J. Feijen, D.W. Grijpma: A Poly(D,Llactide) Resin for the Preparation of Tissue Engineering Scaffolds by Stereolithography. Biomaterials 30 (2009) 3801-3809.
[16] T. Kokubo, H. Takadama: How useful is SBF in predicting in vivo bone bioactivity? Biomaterials (2006) 2907-2915.
[17] M. Emmert, P. Witzela, D. Heinrich: Challenges in tissue engineering – towards cell control inside artificial scaffolds. Soft Matter 12 (2016) 4287-4294.
[18] R. Zhang, P.X. Ma: Porous poly(L-lactic acid)/apatite composites created by biomimetic process. J Biomed Mater Res 45 (1995) 285-293.
[19] K. Zhang, Y. Wang, M.A. Hillmyer, L.F. Francis: Processing and properties of porous poly(L-lactide)/bioactive glass composites. Biomaterials 25 (2004) 2489-2500.

INFLUENCE OF ENVIRONMENTAL FACTORS ON CONTACT LENSES PROPERTIES

Ewa Czerwińska[1], Barbara Szaraniec[1]*, Katarzyna Cholewa-Kowalska[2]

[1] AGH University of Science and Technology, Faculty of Materials Science and Ceramics, Department of Biomaterials and Composites, Al. Mickiewicza 30, 30-059 Krakow, Poland
[2] AGH University of Science and Technology, Faculty of Materials Science and Ceramics, Department of Glass Technology and Amorphous Coatings, Al. Mickiewicza 30, 30-059 Krakow, Poland
* e-mail: szaran@agh.edu.pl

Abstract

Nowadays contact lenses are a very common way of vision correction. To be used successfully, they must meet a number of conditions. This article describes studies on the influence of environmental factors such as low temperature (4°C), high temperature (60°C), various fluids (simulated tear fluid (STF), physiological saline, multi-purpose contact lens solution) and ultraviolet radiation on the properties (wettability, dehydration, UV-vis transmission, surface structure/ microstructure) of 3rd generation silicone hydrogel contact lenses. Contact angle measurement device, gravimetric method (measurement of dehydration), UV-vis spectrophotometry, ATR spectroscopy and SEM microscopy were used during the research. The results showed that environmental factors can influence some features of comfilcon A contact lenses. The reduction of contact lens water content, being the result of a long-term storage at high temperature, might cause changes in their elasticity, thereby sense of discomfort for the user, while storage in physiological saline causes slight decrease in visible light transmission. What is more, the temperature and fluids used for storage of silicone hydrogel contact lenses, as well as ultraviolet radiation affect the microstructure of analysed lenses.

Keywords: *comfilcon A, silicone hydrogel contact lenses, simulated tear fluid (STF), durability, environmental factors*

[Engineering of Biomaterials 144 (2018) 20-27]

Introduction

According to the *American Academy of Ophthalmology*, only in the United States of America, over 150 million of habitants use vision correction methods to correct refractive errors. Almost a quarter of this number are contact lenses users. Contact lenses gained their considerable popularity due to enabling vision correction without introducing noticeable changes in user's appearance and their compatibility with sports lifestyle. There are four main groups of contact lenses: hard contact lenses (usually produced of polymethyl methacrylate (PMMA) or polysilicone acrylate polymers), rigid gas permeable (RGP) contact lenses, hydrogel and silicone hydrogel contact lenses [1]. Thanks to high oxygen permeability and durability silicone hydrogel contact lenses can be used for extended time (up to 30 days), but because of their hydrophobic properties they tend to cumulate proteins on the surface. Their properties are a result of coupling silicone rubber, which facilitates oxygen transport, and hydrogel monomers responsible for movement of a contact lens and fluid transport through lens material. Coupling those monomers in the manner that leads to receiving translucent material is hard, and because of hydrophobic character and quite high stiffness of silicone, it is necessary to use hydrophilic surface coatings or wetting agents [2]. The problem was eliminated in 3rd generation contact lenses which are naturally wettable [3,4]. Improper use of contact lenses (inaccurate cleaning, ignoring the replacement schedule) can cause serious eye infections which might lead to blindness. Even while being used in line with manufacturer's advice contact lenses might be exposed to intensive environmental factors, e.g. being left inside a hot car in summer or at the bathroom's windowsill in winter. Furthermore, contact lenses used during days of high solar insolation, being the outermost layer on the eye, might be affected by a greater influence of UV radiation [5]. The aim of this research is to study the influence of environmental factors, such as low/high temperature, various fluids and UV radiation on the properties (wettability, dehydration, surface roughness, UV-vis transmission spectrum, surface structure and microstructure) of the silicone hydrogel *comfilcon A* contact lenses.

Materials and Methods

Contact lenses and fluids

CooperVision® monthly disposable silicone hydrogel contact lenses (spherical power: -3.75 dioptres, diameter: 14 mm, base curve: 8.6 mm), containing 52% of *comfilcon A* and 48% of water, were used for the study. Being 3rd generation silicone hydrogel contact lenses they are naturally wettable, without need of any additional modifying agents. Aquaform® technology facilitates keeping the water in the lens material and prevents fast dehydration. *Comfilcon A* consists mostly of the following macromers and monomers: NVP, VMA, IBM, TAIC, M3U, FM0411M and HOB (FIG. 1) [6].

After 30 days of use in accordance with the manufacturer's instructions (after use contact lenses were stored in multi-purpose solution - MPS), contact lenses were put into adequate fluids (directly after removing from the eye). Three types of fluids were used in the study:
- EyeCare – multi-purpose solution (MPS) for daily cleaning, disinfecting, protein removing and rewetting of contact lenses. Composition: cleaning agent, hyaluronate, 0.045% HPMC (hydroxypropyl methylcellulose), 0.01% EDTA (*ethylenediaminetetraacetic acid*), 0.00015% PHMB (polyhexamethylene biguanide), buffered isotonic solution;
- physiological saline (0.9% solution of sodium chloride) FRESENIUS;
- simulated tear fluid (STF) – prepared following the composition (TABLE 1) mentioned in the article [8].

Six lenses were put in plastic containers filled with 20 ml of MPS. Three of the containers were placed in the refrigerator and kept at 4°C for a period of one, eight and fifteen days respectively. The remaining three lenses were placed in the laboratory incubator and kept at 60°C for the same period of time. Another three lenses, directly after removing from the eye, were put in MPS, physiological saline and STF and left at room temperature (about 20°C). An additional lens, stored in MPS, was exposed to UV radiation. Dental DTE LUX I Light Cure LED Lamp (850 mW/cm^2~1000 mW/cm^2, 420-480 nm) was used to expose the lens to UV radiation.

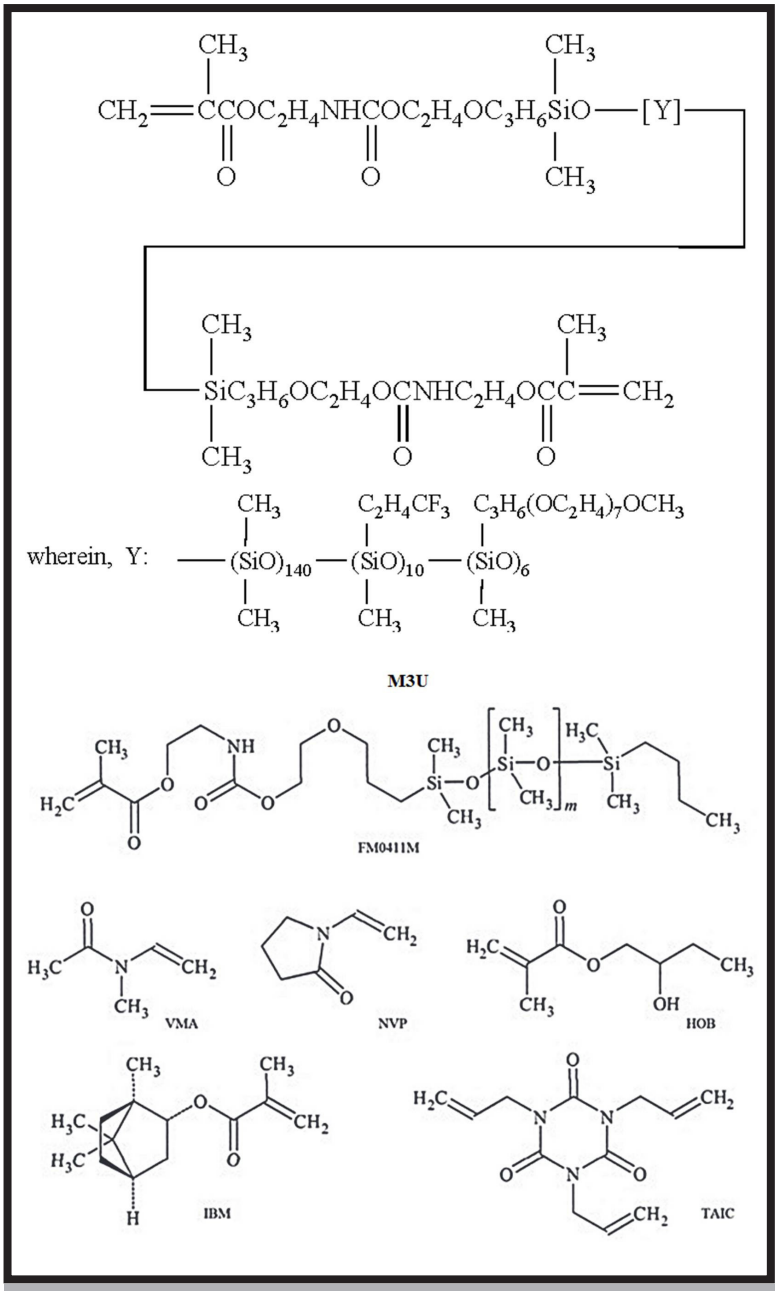

FIG. 1. Comfilcon A principal macromers and monomers: NVP – N-vinyl pyrrolidone; VMA – N-vinyl-N-methylacetamide; IBM - isobornyl methacrylate; TAIC – 1,3,5-triallyl-1,3,5-triazine-2,4,6(1H,3H,5H)-trione; M3U - bis(methacryloyloxyethyl iminocarboxy ethyloxypropyl)-poly(dimethylsiloxane)-poly(trifluoropropylmethylsiloxane)-poly[methoxy-poly(ethyleneglycol] propylmethylsiloxane); FM0411M - methacryloyloxyethyl iminocarboxyethyloxypropyl-poly(dimethylsiloxy)-butyldimethylsilane; HOB – 2-hydroxybutyl methacrylate [6,7].

TABLE 1. Simulated tear fluid composition [8].

Substance	Mass [g] (for 500 ml of solution)
sodium bicarbonate	0.962
potassium chloride	0.555
calcium chloride	0.012
sodium chloride	3.364
albumin	3.345
glucose	0.013

The irradiation was conducted in four 5 seconds cycles with maximal power. The UV irradiance on a sunny, summer day is about 264 mW/m^2 [7], which means that 20 seconds of irradiation using curing light delivering irradiance of 1000 mW/cm^2 (10 000 000 mW/m^2) corresponds to summer light exposure for about 210 h. The reference sample was, depending on the study, a new, unused contact lens or a used contact lens stored in MPS at room temperature.

The lenses wettability was studied with sessile drop technique using KRÜSS DROP SHAPE ANALYSIS SYSTEM DSA 10 Mk2. Surface of the samples was observed using KEYENCE VHX-5000 microscope as well as SEM microscope (NOVA NANO SEM 200) and EDS analysis was conducted (EDS EDAX Detector). Dehydration was assessed using gravimetric method. The study of dehydration was based on mass measurements (precise balance RADWAG WPX 250) of a lens taken out of fluid. The measurement was repeated every 5 min, until the lens was dry (receiving the same results in two subsequent measurements). Optical properties of contact lenses were measured (spectrophotometer UV-vis Jasco V-630, range 200-1100 nm, with 60 mm diameter integrating sphere in the transmission mode) and their surface structure was studied (infrared spectrometer BioRad Excalibur FTS 3000, range 4000-400 cm^{-1}) as well pH of fluid, in which the lenses were stored, was measured with a pH meter ELMETRON CP-411.

Results and Discussions

Wettability

The results obtained by means of sessile drop technique show, that contact angle of a new *comfilcon A* contact lens is 27.4° ± 4.5°, which is in accordance with the literature, which indicates it to be 31.8° [10]. Contact angle of a contact lens that was used and stored in MPS had a very similar value (26.4° ± 4.5°), whereas a lens that was used and stored in STF was characterized by the smallest value (25° ± 2.3°) of contact angle. The greatest contact angle value was measured for a used lens which was stored in physiological saline, which might be a result of sodium chloride crystals deposition on the surface of the lens (FIG. 2). Taking those results into consideration, it can be stated that the type of fluid used for lenses storage have not considerably affected their wettability.

After analyzing contact angle – storage temperature dependency, it can be stated that only after 15 days of storage at 60°C contact angle of the lenses decreased slightly in relation to reference sample (used contact lens stored at room temperature in MPS) (FIG. 3).

The wettability of a contact lens (26.4° ± 4.5°) has not changed after exposure to UV radiation (24.3° ± 5.9°) (FIG. 4). In spite of all the changes in wettability, those being a consequence of storage in various fluids as well as the ones resulting from storage at different temperatures, the surface of the lenses remained highly wettable (Θ <40°).

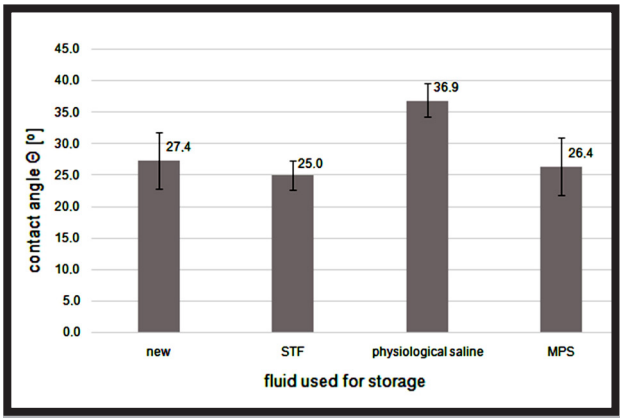

FIG. 2. Changes of the lenses contact angle depending on the fluid used for storage.

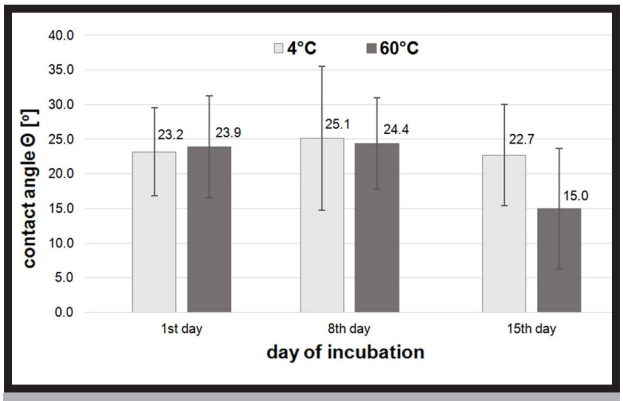

FIG. 3. Changes of the lenses contact angle depending on the storage temperature and incubation time.

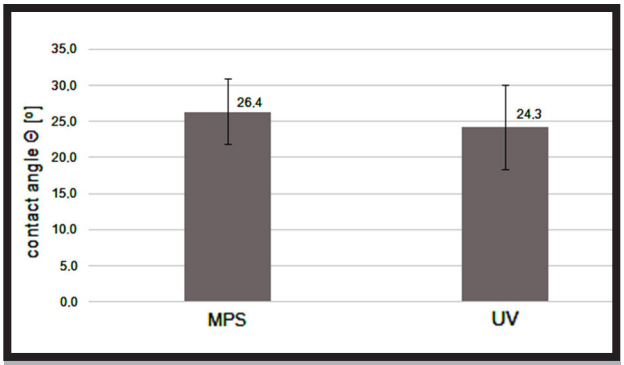

FIG. 4. Changes of the lenses contact angle after exposure to UV radiation.

Digital microscopy

After incubation at 4°C and 60°C the surface of the lenses was observed under a microscope. After 1 day of incubation no changes in transparency of lenses were observed. After 8 days of incubation no changes were observed for a lens kept at 4°C, but the lens kept in 60°C has become slightly opaque.

Dehydration

All the lenses kept in different fluids became dry after the same time (25 min). A used contact lens stored in MPS at room temperature was employed as a reference sample in the study (FIGs. 5-8). No differences were seen in lenses dehydration after storage for one day at 4°C and 60°C (FIG. 5). In the case of lenses incubated at 4°C and 60°C for 8 days (FIG. 6) slight decrease in lenses dehydration could be noticed after being stored at low temperature (after 5 and 20 min from starting the measurement), comparing to the reference sample, but finally all the lenses became dry after 25 min. While analysing dehydration characteristics of lenses kept at 4°C for 15 days, comparing to reference sample, no changes in dehydration time were observed. In the case of a lens kept at 60°C for the same period of time, a decrease in final mass loss value was observed, which can be seen in FIG. 7. The decrease indicates that the lens had a lower water content, which can be an effect of losing some water from the hydrogel network, resulting from a long-term influence of high temperature. After first 5 min it was the surface of the lens that became dry (% of mass loss similar to other samples), whereas afterwards those were the inner layers of the lens. The observation is in accordance with literature data, where the water content changes resulting from a heat disinfection (at above 60°C) are mentioned [11]. Recommendation of avoiding heat disinfection placed by CooperVision® in the product specification is an additional confirmation of observed phenomenon.

No changes were observed in dehydration characteristics of a contact lens exposed to UV radiation in comparison to reference sample (FIG. 8), then it can be stated that UV radiation at the intensity and time of exposure as specified above, does not influence lenses dehydration.

UV-VIS spectrophotometry

Lenses used for the study do not have additional UV filter and allow passing the electromagnetic waves with minimum length of 240 nm, which is in accordance with the literature data [12]. To our best knowledge only one scientific paper concerns evaluation of visible light transmittance of *Comfilcon A* measured by fibre optics spectrometer. The authors noticed that new lenses show the higher visible light transmission (more than 90%) compared to our measurements (not exceed 90%). Also the lens vis transmission declared by supplier is higher (>97%). These differences results mostly from the various equipment used for measurement, and it does not affect our comparative study [13]. Visible range (380-780 nm) transmission spectrum of the contact lens that was stored for 15 days at 60°C is the same as the spectrum of reference sample (new contact lens) (FIG. 9) despite the fact that this sample is a slightly opaque. It will be probably due to measurements protocol, because used integrated sphere allow collecting all passing light. Slightly lowered (by several percent) transmissions of contact lens stored in STF, exposed to UV radiation and subjected to low temperature were registered in the same range. The lowest transmission was registered for a contact lens stored in physiological saline, which can be a result of saline's inability to remove lipid deposits and crystallization of sodium chloride on the surface of the lens. Basing on the vis spectra and the microscopic observation it seems that PBS and also temperature above 40°C are not suitable conditions for storing contact lenses.

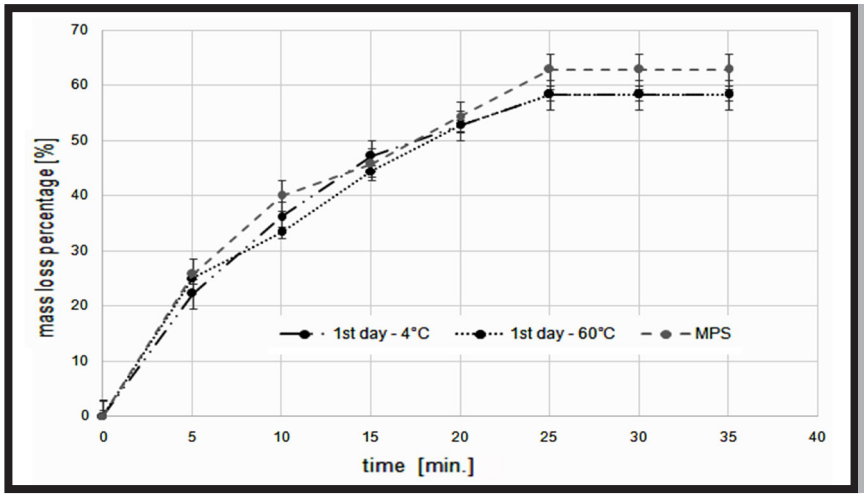

FIG. 5. Dependence of mass reduction on drying time for contact lenses stored for 1 day at 4°C and 60°C.

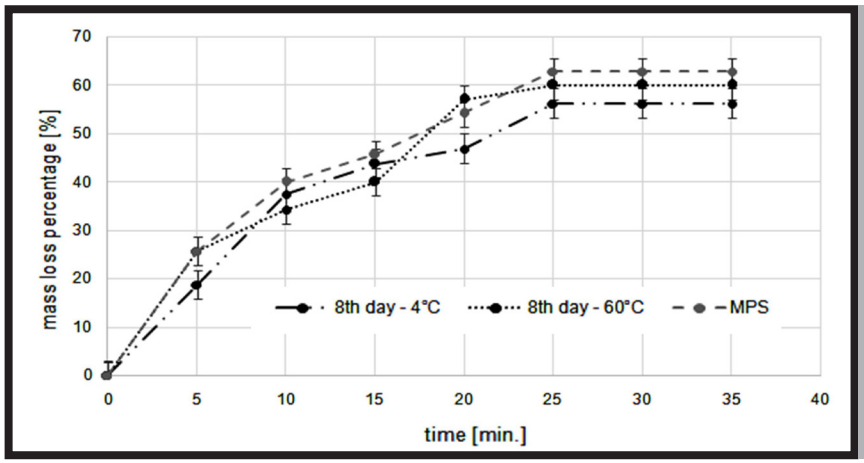

FIG. 6. Dependence of mass reduction on drying time for contact lenses stored for 8 days at 4°C and 60°C.

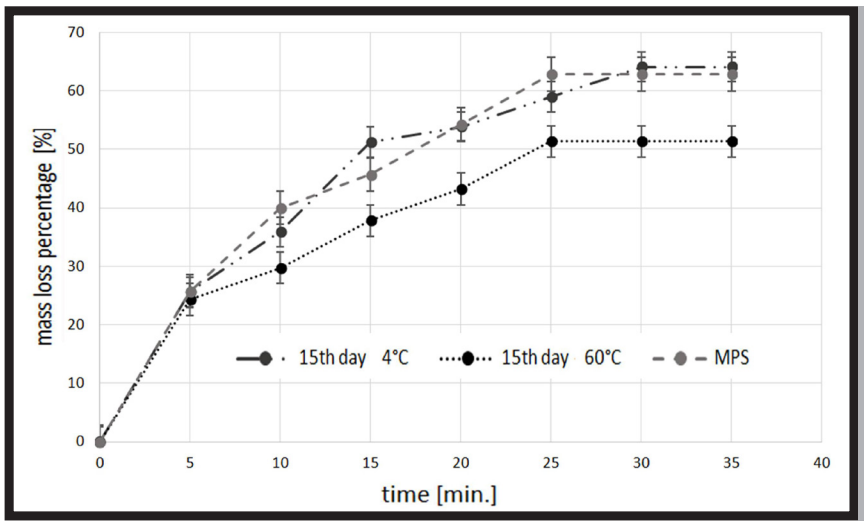

FIG. 7. Dependence of mass reduction on drying time for contact lenses stored for 15 days at 4°C and 60°C.

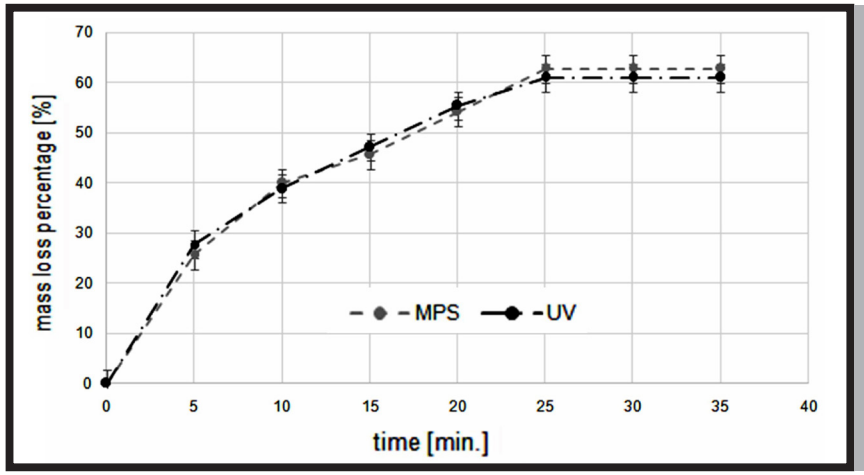

FIG. 8. Dependence of mass reduction on drying time for contact lenses exposed to UV radiation.

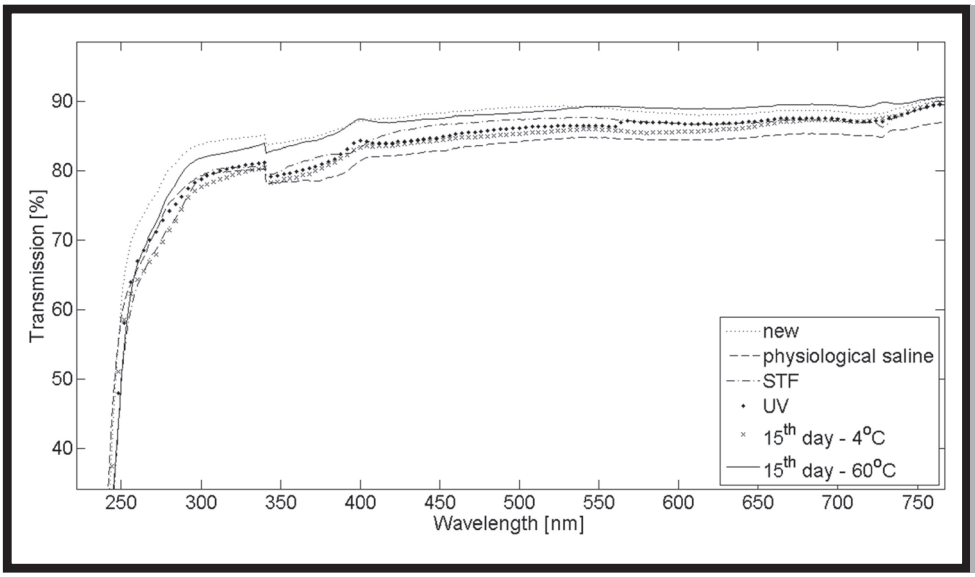

FIG. 9. UV-VIS spectra of contact lenses stored at various environmental conditions.

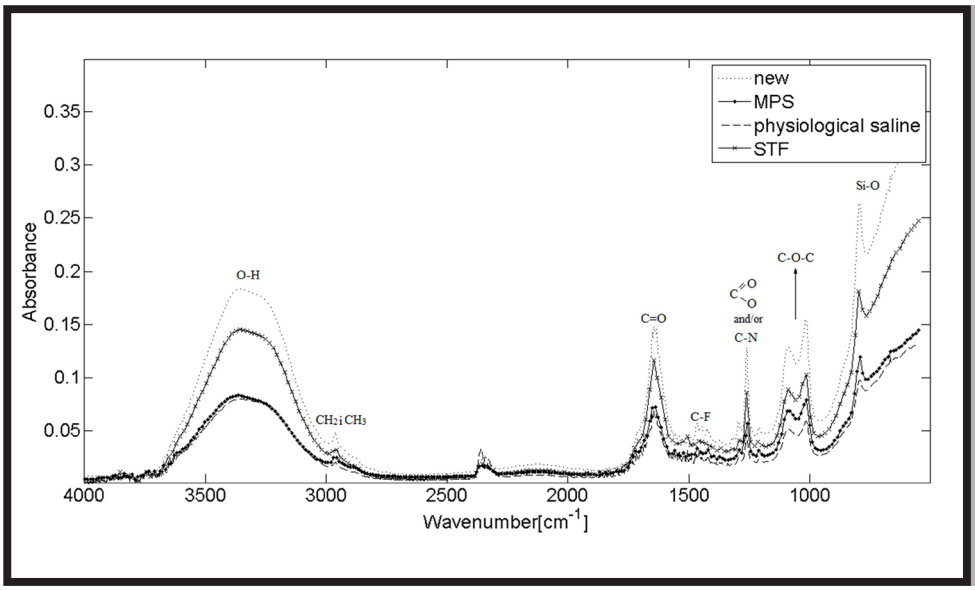

FIG. 10. ATR spectra of contact lenses stored in various fluids.

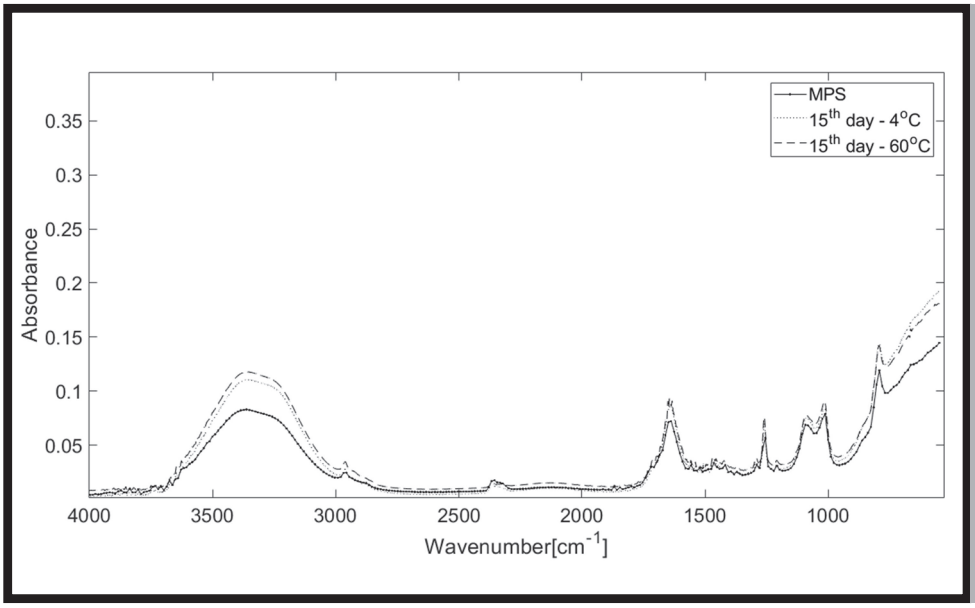

FIG. 11. ATR spectra of contact lenses stored at different temperatures.

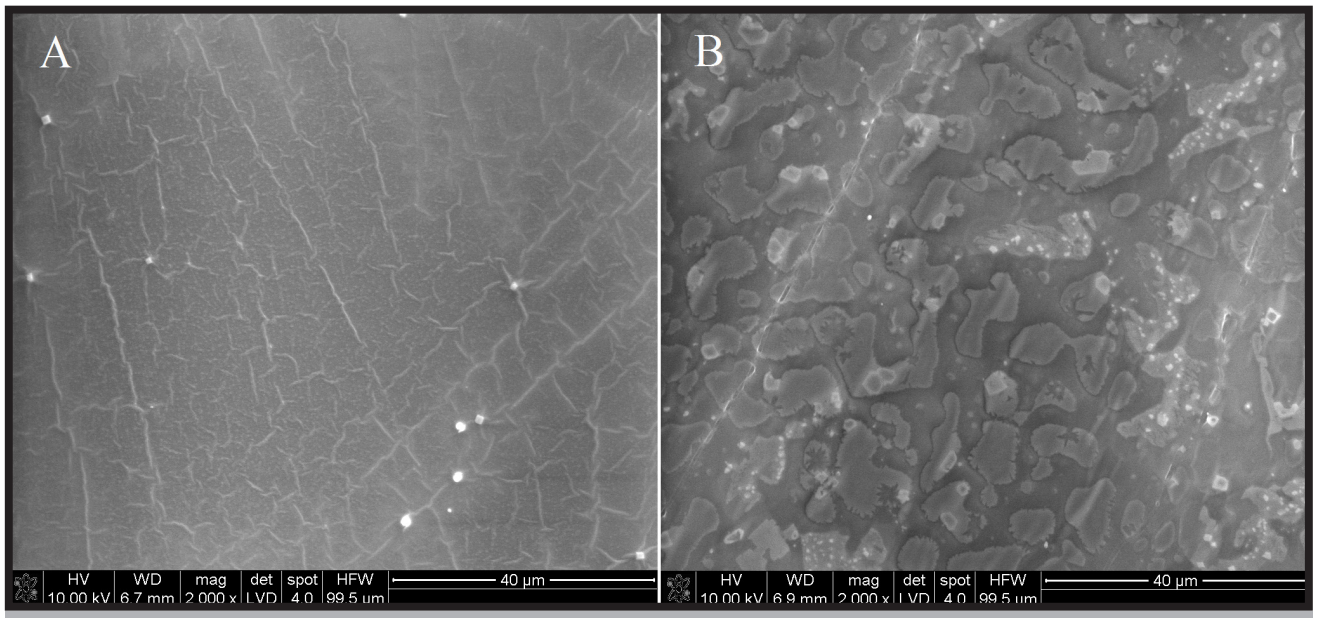

FIG. 12. SEM microphotographs of lenses stored for 1 day at different temperatures (magnification x2000): A) 4°C, B) 60°C.

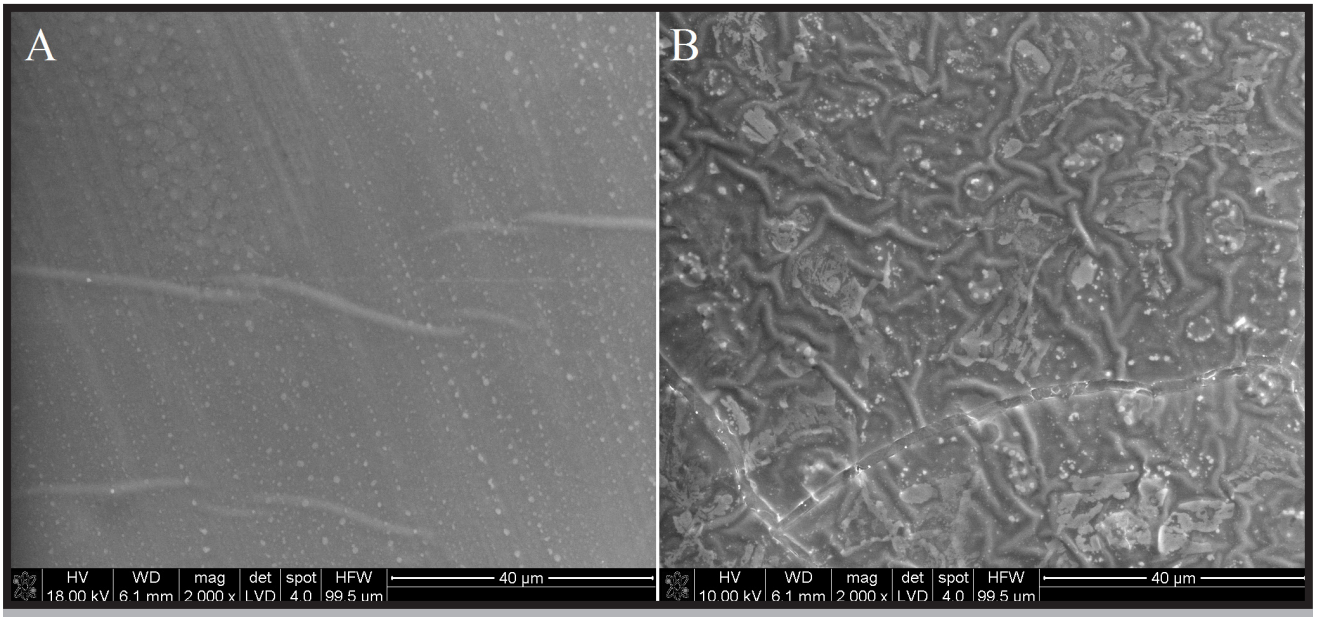

FIG. 13. SEM microphotographs of lenses stored for 8 days at different temperatures (magnification x2000): A) 4°C, B) 60°C.

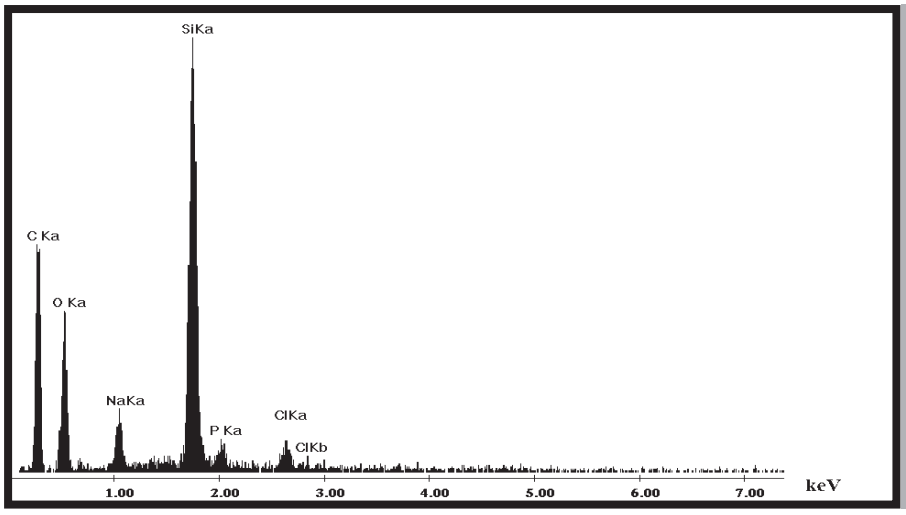

FIG. 14. EDS analysis for a lens stored for 8 days at 60°C.

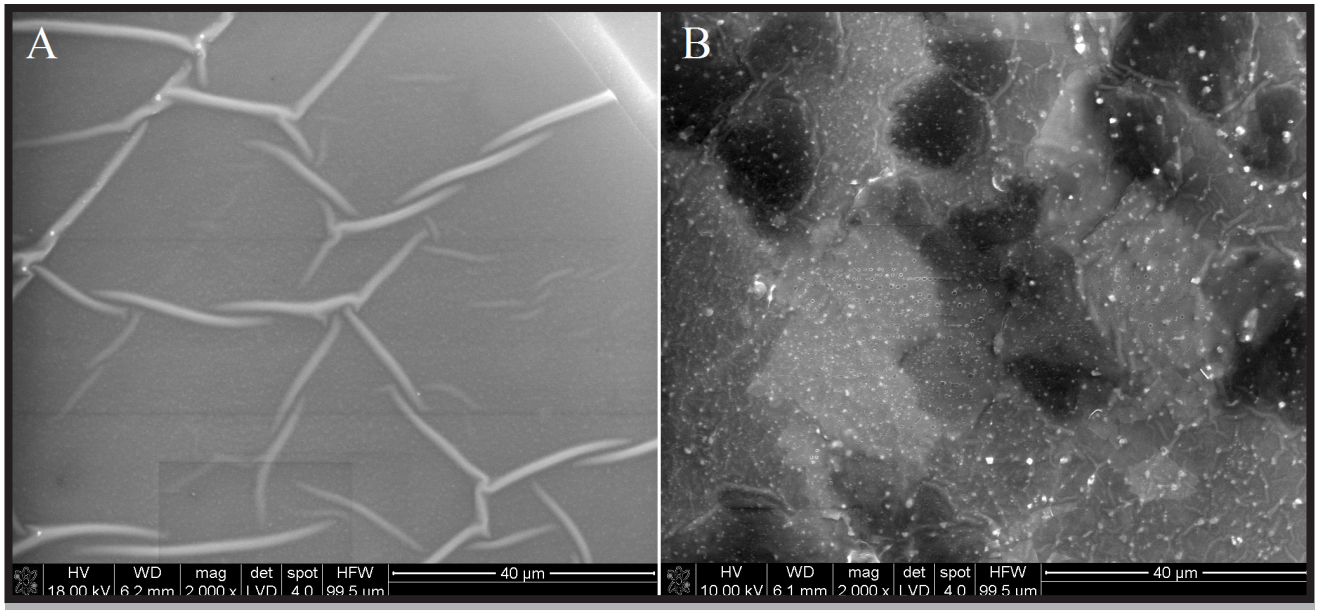

FIG. 15. SEM microphotographs of lenses stored for 8 days at different temperatures (magnification x2000): A) 4°C, B) 60°C.

ATR spectroscopy

Bands characteristic for certain functional groups were identified in the ATR spectra of contact lenses (FIG. 10). In the ATR spectra of contact lenses a band of small intensity was observed at about 1400 cm^{-1}. The band is characteristic for C-F bond, which comes from a small amount of fluorine being a part of M3U (polysiloxane dimethacrylate). M3U is one of the principal macromere components of *comfilcon A* contact lenses [7].

ATR spectra of contact lenses stored at 4°C and 60°C are similar to each other in whole measured range (FIG. 11). What is more, both spectra are very close to the reference sample (used lens stored in MPS at room temperature) spectrum.

It was observed that the relation of particular band's intensity is equal for all studied samples (FIG. 10 and 11), which means that ATR spectra of contact lenses stored in various fluids and at different temperatures did not reveal significant differences between the samples. In all the spectra the same bands, characteristic for functional groups present in *comfilcon A*, can be observed and slight differences in their intensity are so small, that they might be an effect of, e.g. differences in pressing the samples to the crystal. It can be stated that ATR study did not reveal changes in the surface structure of contact lenses after contact with mentioned environmental factors.

Scanning Electron Microscopy

Surface of the lenses was observed using SEM, in order to assess the microstructural changes. Crystals can be seen in SEM microphotographs of lenses stored in physiological saline and MPS. In both cases crystals were identified with EDS analysis as sodium chloride (NaCl). On the surface of a lens stored for 1 day at low temperature small cracks can be observed (FIG. 12). After 8 and 15 days of exposure to 4°C the surface of a lens became smoother between bigger wrinkles (FIG. 13 and FIG. 15). Significant changes were observed on the surface of a lens stored at high temperature. After 1 day of incubation precipitate aggregations showed up on the surface of the lens (FIG. 12) which became bigger after 8 days (FIG. 13). EDS analysis identified it to be phosphorus-containing precipitate (FIG. 14).

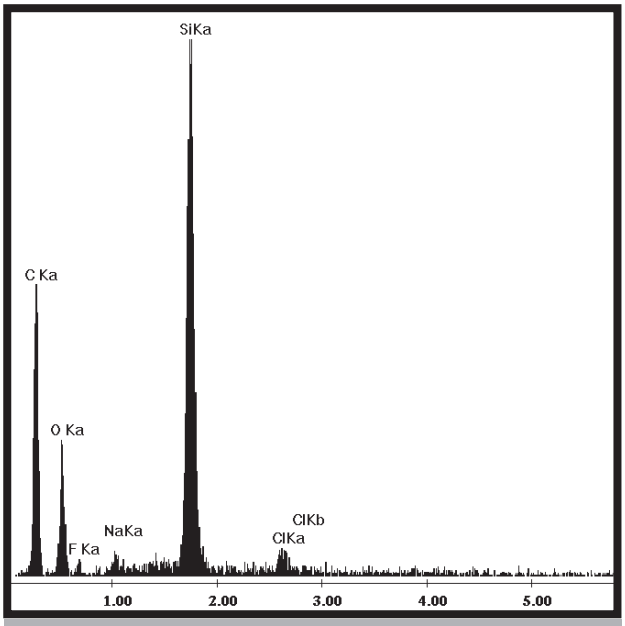

FIG. 16. EDS analysis for a lens stored for 15 days at 60°C.

After 15 days of incubation at 60°C the surface of the lens appears to be worn out, but no precipitation can be observed (FIG. 15) and they are not present in EDS results (FIG. 16). Phosphorus, which was found in the precipitates on the surface of the contact lens, came from MPS which contains buffered isotonic solution (probably phosphate buffered saline).

A dense network of linked cracks showed up on the surface of the lens after UV radiation exposure (FIG. 17). EDS analysis confirmed the presence of fluorine, which was observed in the ATR spectra.

pH measurements

The pH measurements of MPS's in which contact lenses were incubated at 4°C and 60°C did not reveal any significant changes, which means that, during the study, the lenses had not released any factors that would change fluid's pH (FIG. 18).

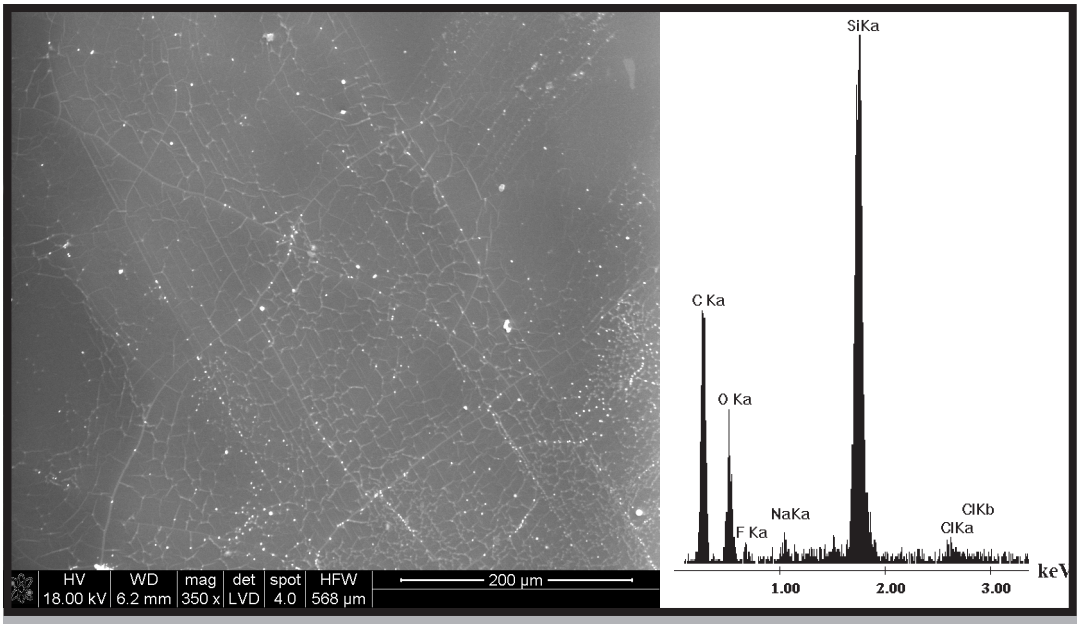

FIG. 17. SEM microphotograph along with EDS analysis of a lens exposed to UV radiation.

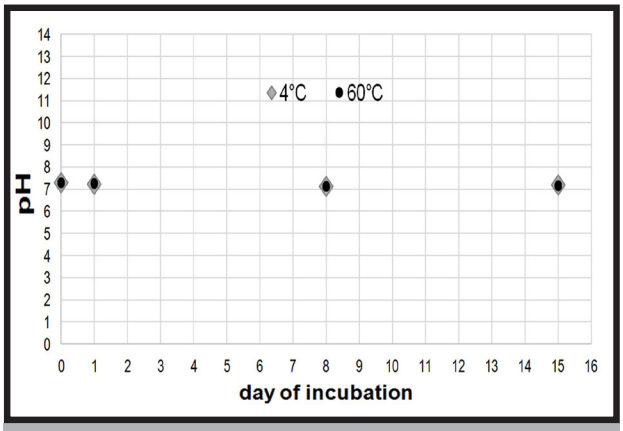

FIG. 18. Changes in MPS's pH after incubation at 4°C and 60°C.

Conclusions

The study conducted on contact lenses stored at 4°C and 60°Cin various fluids and exposed to UV radiation demonstrated that the environmental factors can influence chosen properties of *comfilcon A* contact lenses. A decrease in water content of a contact lens, being a result of a long-term storage at high temperature might cause changes in elasticity of a lens, thereby a sense of discomfort for the user; however, storage of the contact lens in physiological saline is the cause of the reduction of visible light transmission through the lens. What is more, it can be stated that temperature and fluids used for silicone hydrogel contact lenses storage, as well as UV radiation exposure, influence a microstructure of studied lenses. Study of the properties of the lenses before and after contact with various environmental factors showed changes which might influence users' comfort, but not their security.

Acknowledgments

The authors acknowledge financial support from AGH-UST project no 11.11.160.182.

References

[1] Remington J.P., Beringer P.: The Science and Practice of Pharmacy 22nd ed., Pharmaceutical Press, London 2012.
[2] Jones L.: Modern contact lens materials: A clinical performance update. Contact Lens Spectrum 17 (9) (2002) 24-35.
[3] Szczotka-Flynn L.: Looking at Silicone Hydrogels Across Generations, Optometric Management, Issue: May 2008.
[4] Caló E., Khutoryanskiy V.V.: Biomedical applications of hydrogels: A review of patents and commercial products, European Polymer Journal 65 (2015) 252-267.
[5] Behar-Cohen F., Baillet G., Ayguavives T., Ortega Garcia P., Krutmann J., Peña-García P., Reme C., Wolffsohn J.S.: Ultraviolet damage to the eye revisited: eye-sun protection factor (E-SPF®), a new ultraviolet protection label for eyewear, Journal of Clinical Ophthalmology 82 (2014) 87-104.
[6] Filipecki J., Kotynia K., Filipecka K.: Investigation of the Degree of Disorder of the Structure of Polymer Soft Contact Lenses Using Positron Annihilation Lifetime Spectroscopy PALS, Polymers in Medicine 46 (2016) 17-23.
[7] Manesis N.J., Back A.: Silicone Hydrogel Contact Lenses, patent no. US20140200286 A1, filing date: 14.01.2013, publication date: 17.07.2014
[8] Marques M.R.C., Loebenberg R., Almukainzi M.: Simulated Biological Fluids with Possible Application in Dissolution Testing; Dissolution Technologies 18(3) (2011) 15-29.
[9] Meneu J.J.: What's the UV Index and Why Do Smart Clothing Manufacturers Care? Arrow Electronics (2016).
[10] Y.C. Lai, M.T. Yeh, H.Y. Li, W.J. Ting: Silicone hydrogel composition and silicone hydrogel contact lenses made from the composition, patent no. EP 2738221 A1, filing date: 10.06.2013, publication date: 04.06.2014
[11] B. Pankowska, I. Wojciechowska: Contact lenses, Volumed Press, Wrocław 1994
[12] L. Moore, J.T. Ferreira: Ultraviolet (UV) transmittance characteristics of daily disposable and silicone hydrogel contact lenses; Contact Lens & An terior Eye 29 (2006) 115-122.
[13] R. Fuentes, E. Fernández, I. Pascual, C. García: UV-Visible Transmittance of Silicone-Hydrogel Contact Lenses measured with a fiber optic spectrometer Proc. of SPIE Vol. 8785, 8785AZ, 8th Iberoamerican Optics Meeting and 11th Latin American Meeting on Optics, Lasers and Applications.

STUDIA PODYPLOMOWE

Biomateriały – Materiały dla Medycyny

2018/2019

Organizator: Akademia Górniczo-Hutnicza im. Stanisława Staszica w Krakowie Wydział Inżynierii Materiałowej i Ceramiki Katedra Biomateriałów i Kompozytów **Kierownik:** prof. dr hab. inż. Elżbieta Pamuła **Sekretarz:** dr inż. Małgorzata Krok-Borkowicz	**Adres:** 30-059 Kraków, Al. Mickiewicza 30 Pawilon A3, p. 208, 210 lub 501 tel. 12 617 44 48, 12 617 23 38, fax. 12 617 33 71 email: epamula@agh.edu.pl; krok@agh.edu.pl http://www.agh.edu.pl/ksztalcenie/oferta-ksztalcenia/studia-podyplomowe/biomaterialy-materialy-dla-medycyny/

Charakterystyka:
Tematyka prezentowana w trakcie zajęć obejmuje przegląd wszystkich grup materiałów dla zastosowań medycznych: metalicznych, ceramicznych, polimerowych, węglowych i kompozytowych. Słuchacze zapoznają się z metodami projektowania i wytwarzania biomateriałów a następnie możliwościami analizy ich właściwości mechanicznych, właściwości fizykochemicznych (laboratoria z metod badań: elektronowa mikroskopia skaningowa, mikroskopia sił atomowych, spektroskopia w podczerwieni, badania energii powierzchniowej i zwilżalności) i właściwości biologicznych (badania: *in vitro* i *in vivo*). Omawiane są regulacje prawne i aspekty etyczne związane z badaniami na zwierzętach i badaniami klinicznymi (norma EU ISO 10993). Słuchacze zapoznają się z najnowszymi osiągnięciami w zakresie nowoczesnych nośników leków, medycyny regeneracyjnej i inżynierii tkankowej.

Sylwetka absolwenta:
Studia adresowane są do absolwentów uczelni technicznych (inżynieria materiałowa, technologia chemiczna), przyrodniczych (chemia, biologia, biotechnologia) a także medycznych, stomatologicznych, farmaceutycznych i weterynaryjnych, pragnących zdobyć, poszerzyć i ugruntować wiedzę z zakresu inżynierii biomateriałów i nowoczesnych materiałów dla medycyny. Słuchacze zdobywają i/lub pogłębiają wiedzę z zakresu inżynierii biomateriałów. Po zakończeniu studiów wykazują się znajomością budowy, właściwości i sposobu otrzymywania materiałów przeznaczonych dla medycyny. Potrafią analizować wyniki badań i przekładać je na zachowanie się biomateriału w warunkach żywego organizmu. Ponadto słuchacze wprowadzani są w zagadnienia dotyczące wymagań normowych, etycznych i prawnych niezbędnych do wprowadzenia nowego materiału na rynek. Ukończenie studiów pozwala na nabycie umiejętności przygotowywania wniosków do Komisji Etycznych i doboru metod badawczych w zakresie analizy biozgodności materiałów.

Zasady naboru:
Termin zgłoszeń: od 20.09.2018 do 20.10.2018 (liczba miejsc ograniczona - decyduje kolejność zgłoszeń)
Wymagane dokumenty: dyplom ukończenia szkoły wyższej
Osoby przyjmujące zgłoszenia:
prof. dr hab. inż. Elżbieta Pamuła (pawilon A3, p. 208, tel. 12 617 44 48, e-mail: epamula@agh.edu.pl)
dr inż. Małgorzata Krok-Borkowicz (pawilon A3, p. 210, tel. 12 617 23 38, e-mail: krok@agh.edu.pl)

Czas trwania: 2 semestry (od XI 2018 r. do VI 2019 r.) 8 zjazdów (soboty-niedziele) 1 raz w miesiącu	**Opłaty:** 2 600 zł